Examination of Single Crystals: Optical and X-Ray Diffraction Practice

5

5.1 Introduction

The preliminary optical examination of crystalline specimens is interesting and useful in its own right and is a major tool still employed by mineralogists and geologists. However, in structure determinations with modern equipment, it is not uncommon nowadays to by-pass this step and proceed immediately with X-ray studies. This is because in most cases, the X-ray technique is straightforward and data can be quickly scanned with a single-crystal X-ray diffractometer, Sects. 5.5 and 5.6, or with an area detector (see Sect. 5.7), and the suitability and quality of the crystal assessed. There are other situations, however, where complications may arise, for example, because of an unusual crystal habit, Sect. 5.3.5, pseudosymmetry, Sects. 7.2.2, 7.5.4, and Sect. 8.5.3, or twinning, Sect. 5.10. In such cases, it might be possible to extract useful information from an optical examination of a crystal before the more detailed, costly and time-consuming X-ray methods are tried.

5.2 Crystal Growing

It is frequently the case that the crystals supplied for crystallographic work are not suitable for immediate use; then, it is necessary to recrystallize the material in order to obtain specimens appropriate for both X-ray and optical studies.

5.2.1 Growing Crystals for X-Ray Diffraction

In Sect. 10.2ff we give considerable space to the discussion of growing crystals of proteins because this specialized and important process can be difficult. It is, however, equally important to obtain good crystals of inorganic and organic smaller-molecule materials, as the quality of the crystal will influence both the value of an optical investigation and that of the X-ray diffraction data and, thus, of the structure determination itself. Crystals used for X-ray diffraction are commonly of size ranging between 0.1 and 0.5 mm, and crystals of such dimensions are generally obtained by a relatively slow growth process. The slow growth favors the production of crystals that are not twinned (q.v.) or disordered (q.v.), and from which occluded substances, such as dust or solvent molecules are absent, except where the solvent is germane to the crystal structure. There are several techniques that are

M. Ladd and R. Palmer, *Structure Determination by X-ray Crystallography: Analysis by X-rays and Neutrons*, DOI 10.1007/978-1-4614-3954-7_5,

employed in general crystal growing. It is not possible to give strict directions and it is often necessary to vary the conditions of growth in order to obtain satisfactory crystals.

5.2.2 Crystallization from Solution

In this method a suitable solvent must be found, and it is useful to remember that many inorganic materials and organic material containing polar functional groups, such as –OH or $–CO_2H$, for example, will dissolve in water or ethanol. Non-polar molecules frequently dissolve in solvents such as benzene or toluene. In some cases, mixed solvents are an asset. For example, steroid-like substances can often be recrystallized well from a mixture of methanol and dichloromethane.

Sufficient material to form a near-saturated solution may be dissolved in warm solvent in a clean glass vessel protected from direct exposure to the surroundings and allowed to cool slowly. Slow cooling may be achieved by suspending the crystallization vessel in a Dewar flask or by using a thermal reservoir. Many variations on this procedure are possible.

Crystallization from solution is essentially a process of concentration of the solution until crystals begin to form either by cooling a solution of the substance or by slow room-temperature evaporation. If the vessel in which the crystals are to be grown is very smooth-walled, crystallization may need to be induced by rubbing the wall of the vessel with a clean glass rod.

5.2.3 Crystallization by Diffusion

Another technique for bringing about crystallization is by diffusion into the solution of a miscible solvent in which the crystals have a small solubility. Thus, "ibuprofen," α-methyl-4-(2-methylpropyl) benzeneaceticacid ($C_{12}H_{18}O_2$), can be crystallized by diffusion from ethanol/diethylether, and ammonium nitrate (NH_3NO_3) can be crystallized by diffusing ethanol into its aqueous solution.

Crystallization by diffusion may be brought about also by introducing the vapor of the solvent in which the substance is least soluble above the surface of the solution of the substance in a suitable vessel. This technique and the related hanging-drop method are discussed in Sect. 10.2.9, and are not restricted to proteins.

5.2.4 Crystallization by Sublimation

Some materials are suitable for crystallization by sublimation; iodine, I_2, and menthol ($C_{10}H_{20}O$) are substances that can be treated in this manner. In principle, the material is warmed and the vapor allowed to impinge on a cool surface; it can sometimes be advantageous for the material to be under reduced pressure. Not surprisingly, the size of the crystals is governed by the rate of sublimation.

5.2.5 Other Issues

There are materials, particularly inorganic and refractory substances and polymers that cannot be formed into single crystals. They exist as microcrystalline powders of size in the region of 10^{-3} mm, and can rarely be recrystallized to larger dimensions. For this reason, we treat structure determination from powder materials in Chap. 12, where we show that considerable success has been achieved with this X-ray technique.

5.3 Optical Techniques

We discuss first some aspects of the interaction between crystals and two different electromagnetic radiations, light and X-rays. Light, with its longer wavelength (5000–6000 Å) can reveal only limited information about crystal structures, whereas X-rays with wavelengths of less than about 2 Å can be used to determine the relative positions of atoms in crystals. A preliminary examination of a crystal aims to determine its space group and unit-cell dimensions, and is generally carried out by X-ray techniques. However, the optical methods described here are simple but often very effective; they should be regarded as a desirable prerequisite to an X-ray structure determination, particularly where automated intensity measurement is used.

5.3.1 Polarized Light

An ordinary light source emits wave trains, or pulses of light, vibrating in all directions perpendicular to the direction of propagation, as shown in Fig. 5.1; the light is said to be unpolarized. The vibrations of interest to us are those of the electric vector associated with the waves. Any one of these random vibrations can be resolved into two mutually perpendicular components, and the resultant vibration may, therefore, be considered as the sum of all components in these two perpendicular directions. In order to study the optical properties of crystals, we need to restrict the resultant vibration of the light source to one direction only by eliminating the component at right angles to it.

A polarizer (*P*), consisting of a sheet of Polaroid, transmits light vibrating in the horizontal direction *LM* and absorbs all components vibrating in the direction perpendicular to *LM*. Thus, light passing through the polarizer vibrates in one plane only, and is said to be plane-polarized. The plane contains the vibration direction that is perpendicular to the direction of propagation and to the direction of propagation itself. A second Polaroid, the analyzer (*A*), is placed after the polarizer and rotated so that its vibration transmission direction (*MN*) is at 90° to that of the polarizer. It receives no component parallel to its transmission direction and, therefore, absorbs all the light transmitted by the polarizer. The two Polaroids are then said to be crossed. This effect may be demonstrated by cutting a Polaroid sheet marked with a straight line *LMN* into two sections, *P* and *A*. When superimposed, the two halves will not transmit light if the reference lines (vibration directions) *LM* and *MN* are exactly perpendicular, or *crossed*. In intermediate positions, the intensity of light

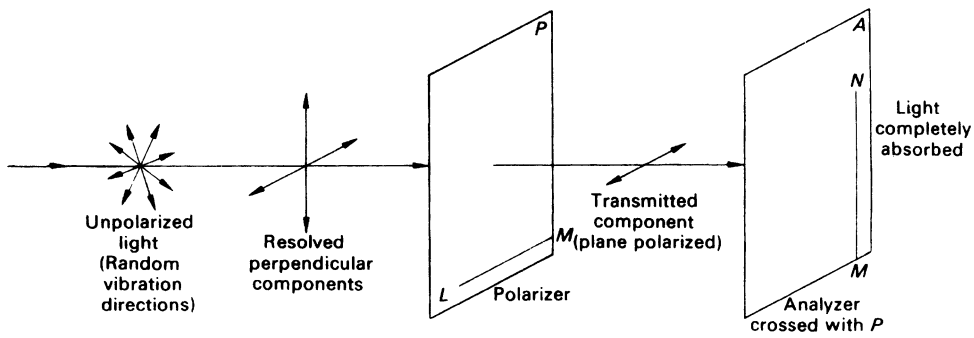

Fig. 5.1 Production of plane-polarized light by passing unpolarized light through a sheet of Polaroid film (the polarizer, *P*). A second, identical sheet of Polaroid (the analyzer, *A*), rotated through 90° with respect to *P*, completely absorbs all light transmitted by *P*. The lines *LM* and *MN* were parallel on the sheet from which *P* and *A* were cut

Table 5.1 Crystal directions readily derivable from an optical study

Optical classification	Crystal system	Information relating to crystal axes likely to be revealed
Isotropic	Cubic	Axes may be assigned from the crystal morphology
Anisotropic, uniaxial	Tetragonal Hexagonal Trigonal[a]	Direction of the z axis Direction of the z axis Direction of the z axis
Anisotropic, biaxial	Orthorhombic Monoclinic Triclinic	Direction of at least the x, y, or z axis, possibly all three axes Direction parallel to the y axis No special relationship between the crystal axes and the vibration directions

[a]Referred to hexagonal axes

transmitted varies from a maximum, where they are parallel, to zero (in the crossed position). The production and use of plane-polarized light by this method is used in the polarizing microscope.

5.3.2 Optical Classification of Crystals

Crystals may be grouped, optically, under two main headings: isotropic crystals and anisotropic, or birefringent, crystals. All crystals belonging to the cubic system are optically isotropic: the refractive index of a cubic crystal is independent of the direction of the light incident upon it, and its optical characteristics are similar to those of glass. Non-cubic crystals exhibit a dependence on direction in their interaction with light.

Anisotropic crystals are divided into two groups: uniaxial crystals, which have one optically isotropic section and include the tetragonal, hexagonal, and trigonal crystal systems, and biaxial crystals, which have two optically isotropic sections and belong to the orthorhombic, monoclinic, or triclinic crystal systems.

A preliminary optical examination of a crystal will usually show whether it is isotropic, uniaxial, or biaxial. Distinction between the three biaxial crystal systems is often possible in practice and, depending on how well developed the crystals are, a similar differentiation may also be effected for the uniaxial crystals. Even if an unambiguous determination of the crystal system is not forthcoming, the examination should, at least, enable the principal symmetry directions to be identified; Table 5.1 summarizes this information.

5.3.3 Uniaxial Crystals

As an example of the use of the polarizing microscope, we consider a tetragonal crystal, such as potassium dihydrogen phosphate (KH_2PO_4), lying on a microscope slide with its y axis parallel to the axis of the optical path through a microscope, illustrated in Fig. 5.2. The microscope is fitted with a polarizer (P), and an analyzer (A) which is crossed with respect to P and may be removed from the optical path. The crystal can be rotated on the microscope stage between P and A. With the Polaroids crossed and no crystal in between, the field of view is uniformly dark. However, with the crystal interposed, this situation will not necessarily be obtained.

The tetragonal crystal is lying with its (010) plane on the microscope slide; both the x and z axes are, therefore, perpendicular to the microscope axis. In general, some of the light passing through the crystal will be transmitted by the analyzer, even though P and A are crossed. The intensity of the transmitted light varies as the crystal is rotated on the microscope stage between the polarizer and the analyzer. During a complete revolution of the stage, the intensity of transmitted light passes through four maxima

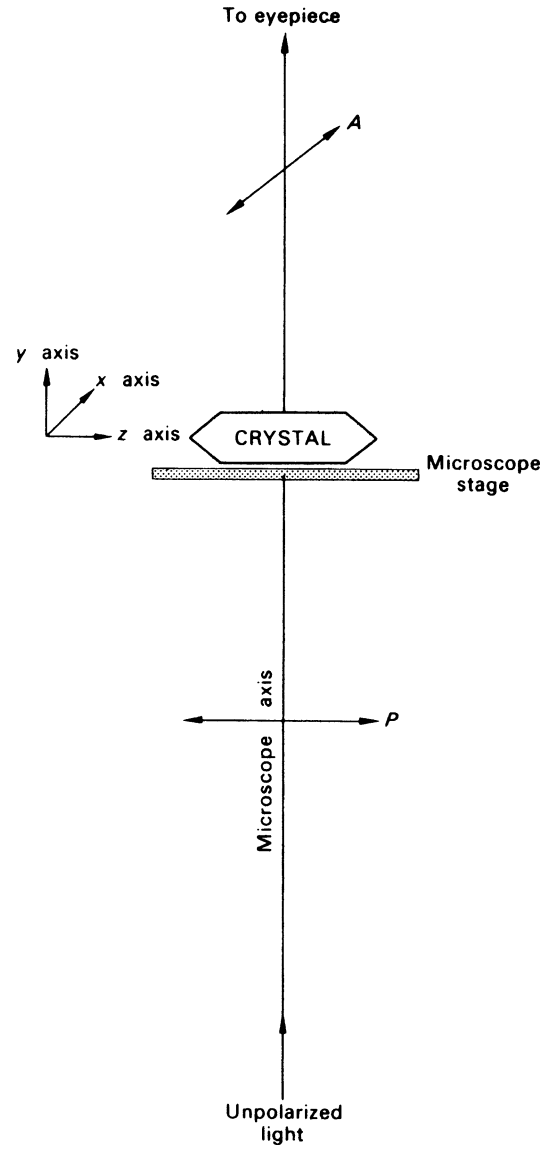

Fig. 5.2 Schematic experimental arrangement for examining extinction directions. A tetragonal crystal is shown on the microscope stage, and the incident light is perpendicular to the z axis of the crystal

and four minima. At the minimum positions, the crystal is usually only just visible. These positions are called *extinction* positions, and they occur at exactly 90° intervals of rotation. Maximum intensity is observed with the crystal at 45° to these directions.

These changes would be observed if the crystal itself were replaced by a sheet of Polaroid. Extinction would occur when the vibrations of the "crystal Polaroid" were perpendicular to those of P or A. A simple explanation of these effects is that the crystal behaves as a polarizer. Incident plane-polarized light from P is resolved by the crystal into two perpendicular components, Fig. 5.3. In the tetragonal crystal, the vibration directions associated with this polarizing effect are parallel to its x and z axes. Rotating the crystal on the microscope stage will, therefore, produce extinction whenever x and z are parallel to the vibration directions of P and A. The x and z axes of a tetragonal

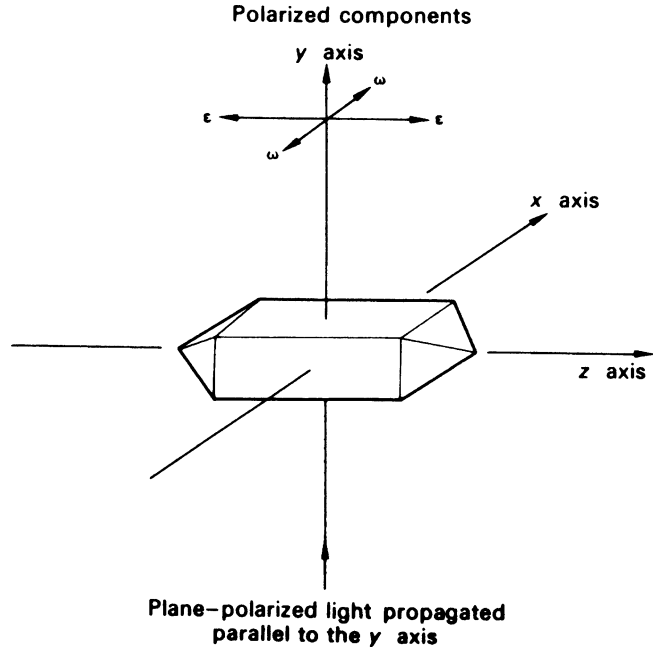

Fig. 5.3 Resolution of incident light into components vibrating parallel to the x and z axes of a tetragonal crystal lying with its y axis parallel to the incident beam; ω and ε are the refractive indices for light vibrating, respectively, perpendicular and parallel to z

crystal correspond to its extinction directions: it should be remembered that the x and y directions are equivalent under the fourfold symmetry of the crystal.

5.3.4 Birefringence

The vibration components produced by a crystal are associated with its different refractive indices. With reference to Fig. 5.3, a tetragonal crystal in light vibrating parallel to the fourfold symmetry axis (z) has a refractive index ε, whereas light vibrating perpendicular to z has a different refractive index, ω; the crystal is said to be *birefringent*, or optically anisotropic. Figure 5.4 represents plane-polarized light incident in a general direction with respect to the crystallographic axes. It is resolved into two components, one with an associated refractive index ω and the other with an associated refractive index ε', both vibrating perpendicular to each other and to the direction of incidence. In general, the value of ε' lies between those of ω and ε.

Two special cases arise: one, already discussed, where the incident light is perpendicular to z, for which $\varepsilon' = \varepsilon$, and the other where the incident light is parallel to z, for which $\varepsilon' = \omega$. It follows that where the direction of incidence is parallel to the z axis, the refractive index is always ω for any vibration direction in the xy plane. Plane-polarized light incident parallel to the z axis will pass through the crystal unmodified. In this particular direction, the crystal is optically isotropic, and if rotated on the microscope stage between crossed Polaroids, it remains in extinction. The z direction of a uniaxial crystal is called the *optic axis*, and there is only one such direction in the crystal; it is the fourfold symmetry axis in the example that we are using.

Identification of the z Axis of a Uniaxial Crystal

A polarizing microscope is usually fitted with eyepiece cross-wires arranged parallel and perpendicular to the vibration directions of the polarizer, and therefore we can relate the crystal vibration

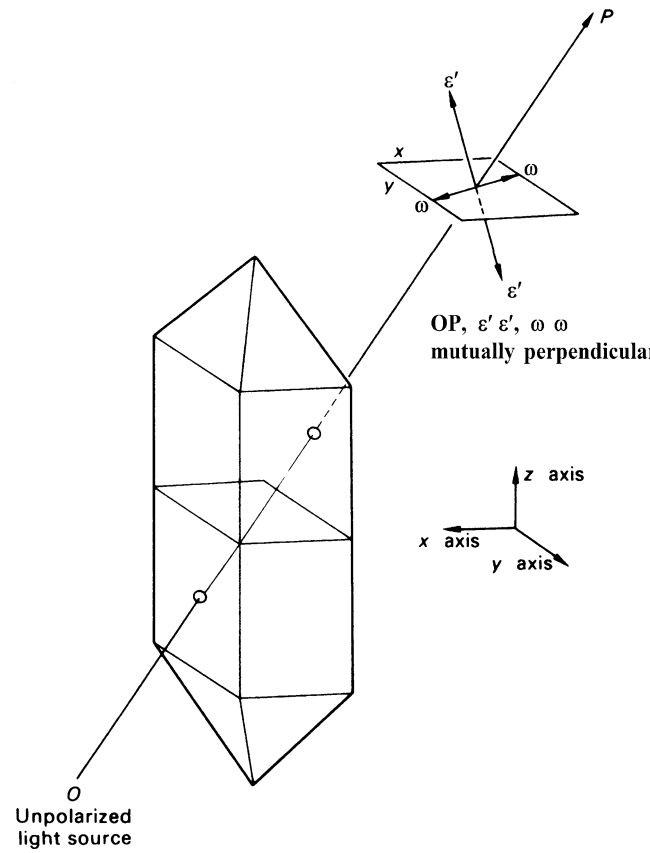

Fig. 5.4 Uniaxial crystal showing a light ray *OP* resolved into two components. One component, with refractive index ω, vibrates in the *xy* plane, the other, with refractive index ε', vibrates parallel to both ω and the ray direction

directions to its morphology. There are two important optical orientations for a tetragonal crystal, namely with the *z* axis either perpendicular or parallel to the axis of the microscope. These orientations are, in fact, important for all uniaxial crystals, and will be described in more detail.

z Axis Perpendicular to the Microscope Axis

In this position, shown by Fig. 5.5, a birefringent orientation is always presented to the incident light beam. Extinction will occur whenever the *z* axis is parallel to a cross-wire, no matter how the crystal is rotated, or flipped over, while keeping *z* normal to the microscope axis. The success of this operation depends to a large extent on having a crystal with well-developed (*hk*0) faces. The term *straight extinction* is used to indicate that the field of view is dark when a crystal edge is aligned with a cross-wire. A face of a uniaxial crystal for which one edge is parallel to *z*, an (*hk*0) face or to its trace on a crystal face, such as (*h*0*l*), will show straight extinction.

z Axis Parallel to the Microscope Axis

The crystal now presents an isotropic section to the incident light beam, and will remain extinguished for all rotations of the crystal, while keeping *z* along the microscope axis. A reasonably thin section of the crystal is required in order to observe this effect. Because of the needle-shaped habit of the crystal, it is necessary to cut the crystal carefully so as to obtain the desired specimen, Sect. 5.10.1.

The section of a uniaxial crystal normal to the *z* axis, if well developed, may provide a clue to the crystal system. Tetragonal crystals often have edges at 90° to one another, whereas hexagonal and

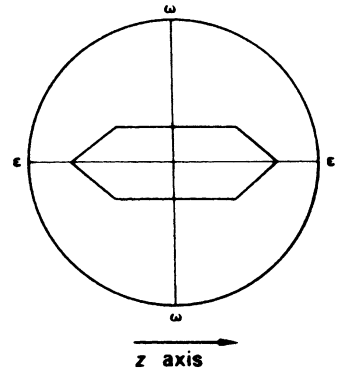

Fig. 5.5 Extinction position for a tetragonal crystal lying with its z axis parallel to the microscope slide. Any [UV 0] direction could be parallel to the microscope axis; extinction will always be straight with respect to the z axis or its trace

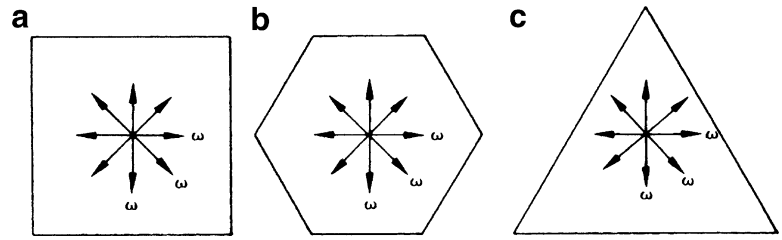

Fig. 5.6 Idealized uniaxial crystals as seen along the z axis. (**a**) Tetragonal. (**b**) Hexagonal. (**c**) Trigonal. The refractive index for light vibrating perpendicular to the z axis is given the symbol ω, and the crystals appear isotropic in this orientation

trigonal crystals often exhibit edges at 60 or 120° to one another. These angles are external manifestations of the internal symmetry; idealized uniaxial crystal sections are shown in Fig. 5.6.

5.3.5 Biaxial Crystals

Biaxial crystals have two optic axes and, correspondingly, two isotropic directions. The reason for this effect lies in the low symmetry associated with the orthorhombic, monoclinic, and triclinic systems, which, in turn, results in less symmetric optical characteristics. Biaxial crystals have three principal refractive indices, n_1, n_2, and n_3 (normally, $n_1 < n_2 < n_3$), associated with light vibrating parallel to three mutually perpendicular directions in the crystal. The optic axes that derive from this property are not necessarily directly related to the crystallographic axes. We shall not concern ourselves here with a detailed treatment of the optical properties of biaxial crystals, but will concentrate on relating the extinction directions to the crystal symmetry.

Orthorhombic Crystals

In the orthorhombic system, the vibration directions associated with n_1, n_2, and n_3 are parallel to the crystallographic axes, but any combination of x, y, and z with n_1, n_2, and n_3 may occur. Consequently, recognition of the extinction directions facilitates identification of the directions of the crystallographic axes. For a crystal with x, y, or z perpendicular to the microscope axis, the extinction, directions will be either parallel or perpendicular to the axis in question, as illustrated in Fig. 5.7.

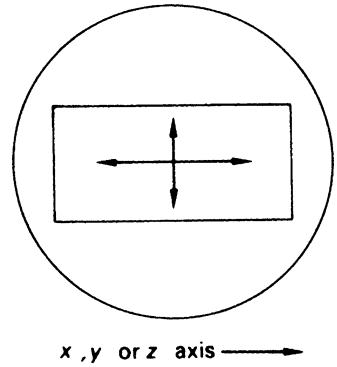

Fig. 5.7 Extinction directions in an orthorhombic crystal viewed along the x, y, or z axis

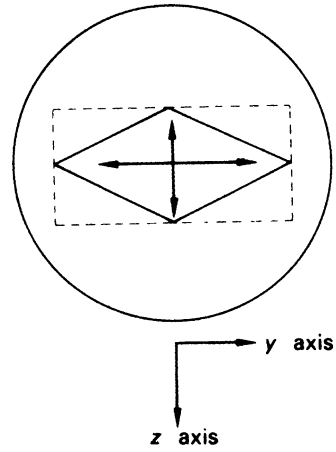

Fig. 5.8 Extinction directions as seen along the x-axis of an orthorhombic crystal with {011} development: an example of symmetric extinction

If the crystal is a well-developed orthorhombic prism, the three crystallographic axes may be identified by this optical method. A common alternative habit of orthorhombic crystals has one axis, x, for example, as a needle axis with the {011} form prominent. The appearance of such a crystal viewed along x is shown in Fig. 5.8, and is an example of a *symmetric* extinction.

Monoclinic Crystals

The lower symmetry of monoclinic crystals results in a corresponding modification of the optical properties in this system. The symmetry axis y is, conventionally, set parallel to one of the vibration directions; x and z are related arbitrarily to the other two mutually perpendicular vibration directions. Hence, two directions are of importance in monoclinic crystals, namely, perpendicular to and parallel to the y axis.

When viewed between crossed Polaroids, a monoclinic crystal lying with its y axis perpendicular to the microscope axis will always show straight extinction, with the cross-wires parallel (and perpendicular) to y. Often, the y axis is a well-developed needle axis; rotation of the crystal about this axis while keeping it perpendicular to the microscope axis will not cause any change in the position of extinction, Fig. 5.9.

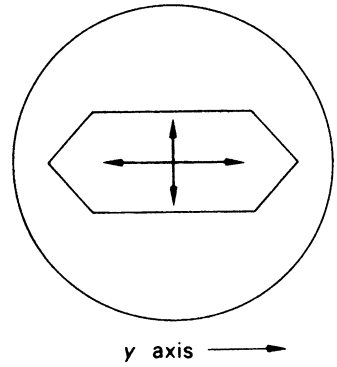

Fig. 5.9 Extinction directions in a monoclinic crystal viewed perpendicular to the *y* axis: an example of straight extinction

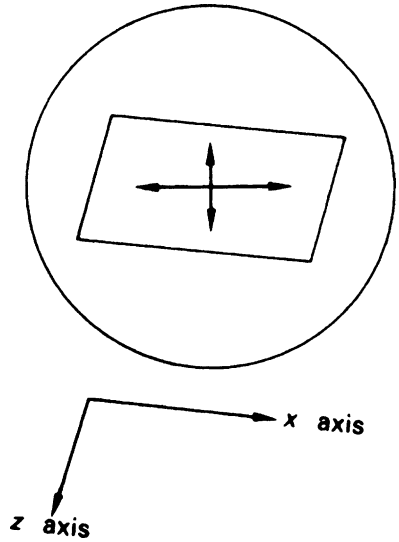

Fig. 5.10 Extinction directions in a monoclinic crystal viewed along the *y* axis—an example of oblique extinction. If the forms developed are pinacoids, that is, {100}, {010}, and {001}, then the *extinction angle*; the angle between a crystal edge and a cross-wire will be related in a simple way to the β angle

If the monoclinic crystal is arranged so that *y* is parallel to the microscope axis, the (010) plane will lie on the microscope slide. Extinction in this position will, in general, be *oblique*, as shown in Fig. 5.10, thus giving further evidence for the position of the *y*-axis direction. The appearance of extinction in a monoclinic crystal in this orientation may be somewhat similar to that of an orthorhombic crystal showing prominent {011} development, compare Figs. 5.8 and 5.10, and confusion may sometimes occur in practice.

Triclinic Crystals

The mutually perpendicular vibration directions associated with n_1, n_2, and n_3 are arbitrarily related to the crystallographic axes, which are selected initially from morphological and X-ray studies.

Reference to Table 5.1 should now enable the reader to consolidate the ideas presented in the discussion of extinction directions in the seven crystal systems. Although it gives only limited

information on the optical properties of crystals, a practical study of a crystal along these lines can often provide useful information about both its system and its axial directions. Further details on the optical properties of crystals may be found in standard works on this subject [1].

5.4 Single-Crystal X-Ray Diffraction Techniques: Intensity Data Collection

With the development of sophisticated X-ray diffractometers, there has been a distinct move away from traditional photographic methods of recording diffraction patterns of crystals, although they still have a value for displaying a picture of the reciprocal lattice, and for investigating the symmetry or perfection of crystals. The introduction of various types of area detectors swings methodology away from the serial, "one reflection at a time," diffractometer toward image-plate principles, reminiscent of the earlier photographic techniques. An understanding of Laue and X-ray oscillation photography and the related geometry is invaluable to those taking the almost inevitable step of progressing from in-house facilities to the use of the synchrotron. The precession camera [2, 3] is sadly no longer used per se but was historically a brilliant innovation that allowed undistorted records of the weighted reciprocal lattice, Sect. 3.4.2, to be produced as a matter of routine. Figure 5.11a, b show zero-level and first-level precession photographs of the orthorhombic crystal of trypsin. Such records can however now be produced from intensity data files using software such as that of Bruker AXS (XPREP/RLATT) [4] thus preserving the art of recording the undistorted reciprocal lattice, Fig. 5.11c.

Over the past 15 years, the role of powder crystallography has been transformed from one of very minor use in structure analysis to one in which it is rapidly becoming a major alternative choice. Chap. 12 provides details of the advances that have taken place to revolutionize this method, while the present chapter discusses the interpretation of the X-ray diffraction data recording techniques in current use for single crystals and methods for the *n* data.

5.4.1 Laue Method

The three variables in the Bragg equation provide a basis for the interpretation of X-ray crystallographic experiments. In the Laue method, Fig. 5.12, the Bragg equation is satisfied by effectively varying λ, utilizing a beam of continuous (white) radiation. Since the crystal is stationary with respect to the X-ray beam, it acts as a sort of filter, selecting the correct wavelength for each reflection according to the Bragg equation.

The diffraction spots on a Laue photograph lie on ellipses, all of which have one end of their major axis at the center of the photographic film, Fig. 5.13. All spots on one ellipse arise through reflections from planes that lie in one and the same zone. In Fig. 5.14, a zone axis for a given Bragg angle θ is represented by ZZ'. A reflected ray is labeled R, and we can simulate the effect of the zone by imagining the crystal to be rotated about ZZ', taking the reflected beam with it. Rays such as R, generate a cone, coaxial with ZZ' and with a semivertical angle θ. The lower limit, in the diagram, of R is the direction (XY) of the X-ray beam, and the general intersection of a circle with a plane (the flat film) is an ellipse. Hence, we can understand the general appearance of the Laue photograph shown in Fig. 5.13. On each ellipse, discrete spots appear instead of continuous bands because only those orientations parallel to zone axes, such as ZZ', that exist for actual crystal planes can give rise to X-ray reflections.

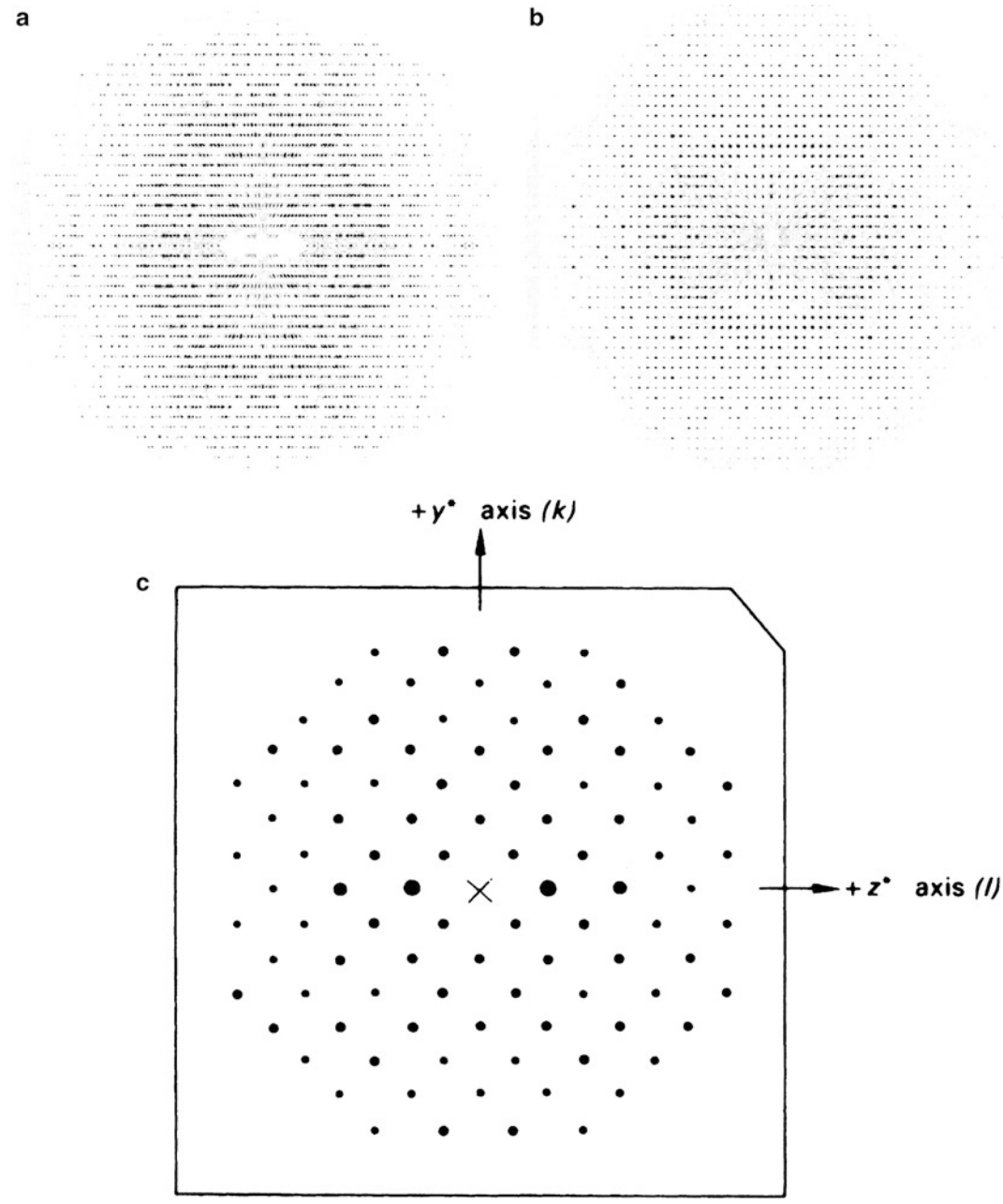

Fig. 5.11 Precession photographs. (**a**) A zero-level precession photograph of an orthorhombic protein crystal, trypsin: $a = 41.5444$, $b = 113.4716$, $c = 50.7156$, space group $P2_12_12$. (**b**) The first-level photograph of the same crystal. (**c**) A simulated precession photograph of an orthorhombic crystal precessing about a (Cu $K\alpha$, $\lambda = 1.5418$ Å). The undistorted, weighted reciprocal lattice zero level is shown; it enables b^*, c^*, and α^* to be measured directly from the film. The lengths b^* and c^* are magnified by the crystal-to-film distance of 60.00 mm, and the diagram has been scaled down by a factor of 0.415 (from the original photograph). By direct measurement on the film, $14b^*$ and $14c^*$ are 67.9 and 68.5 mm, respectively. Hence, $b* = (67.9/0.415)/(60 \times 14) = 0.1948$. Similarly, $c^* = 0.1965$. Thus, $a = 7.91$ Å, $b = 7.84$ Å and $\gamma = 90°$

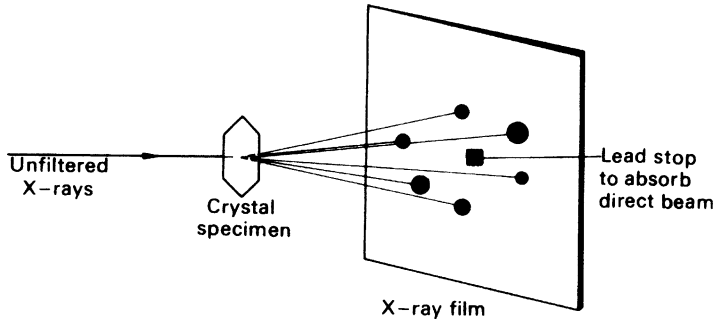

Fig. 5.12 Schematic experimental arrangement for taking a Laue photograph on a flat-plate film

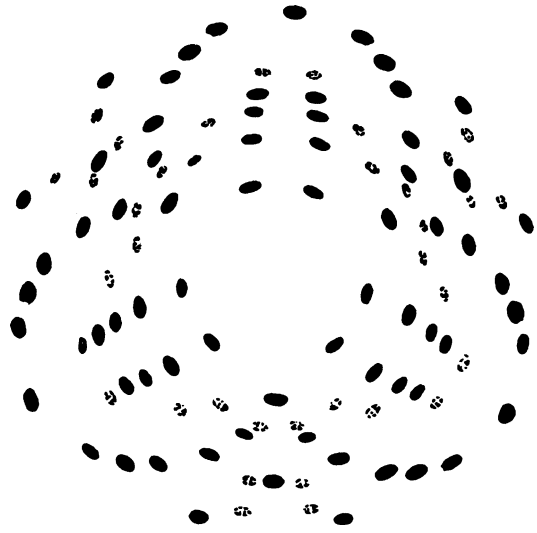

Fig. 5.13 Sketch of a Laue photograph of α-Al_2O_3; the threefold symmetry direction is normal to the photograph (along the X-ray beam)

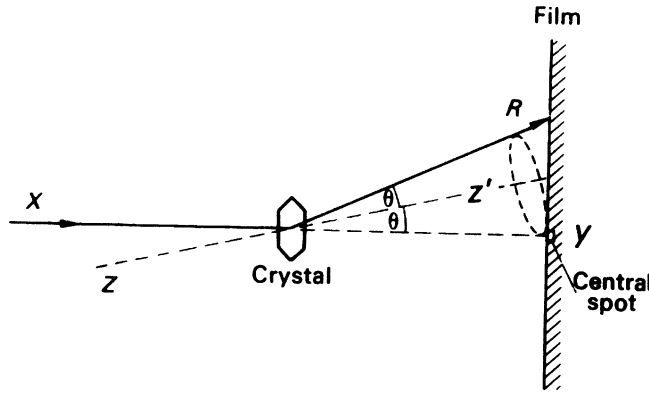

Fig. 5.14 Geometry of the Laue method: XY, X-ray beam direction; ZZ', a zone axis; R, generator of the cone of diffracted rays of semi-angle θ, the Bragg angle; Y, central spot on the film and extremity of the major axis of the ellipse formed by the intersection of the cone with the film

5.4.2 Symmetry in Laue Photographs

One of the useful features of Laue photographs is the symmetry observable on them. The crystal orientation with respect to the X-ray beam is selected by the experimenter from morphological and optical considerations. This orientation, together with the crystal point group, controls the symmetry on the Laue photograph.

In practice, a complication arises by the introduction of a center of symmetry into an X-ray diffraction pattern, in normal circumstances, whether or not the crystal is centrosymmetric. This situation is embodied in Friedel's law, the theoretical grounds for which have been discussed in Sect. 3.6.1. As a result of this law, the diffraction pattern may not reveal the true point-group symmetry of a crystal. It may be recalled that Table 1.6 shows the classification of the 32 crystallographic point groups according to Laue diffraction symmetry.

It cannot be over emphasized that the Laue group assigned to a crystal describes the symmetry of the *complete* X-ray diffraction pattern from that crystal. No single X-ray photograph can exhibit the complete diffraction symmetry, only that of a selected portion which is a projection on to the film, along the direction of the X-ray beam, of the symmetry information that would be encountered in that direction in a crystal having the Laue group of the given crystal.

It follows that in the triclinic system, no symmetry higher than 1 is ever *observable* on a Laue photograph. In other crystal systems, the Laue-projection symmetry depends on the orientation of the crystal with respect to the X-ray beam. Rotation axes of any order reveal their true symmetry when the X-ray beam is parallel to the symmetry axis. Even-order rotation axes, 2, 4, or 6, give rise to mirror diffraction symmetry in the plane normal to the rotation axis when the X-ray beam is normal to that axis. A mirror plane itself shows *m* symmetry parallel to the mirror plane when the X-ray beam is contained by the plane. Various combinations of these effects may be observable, depending upon the Laue group in question.

The nature of the X-ray results, supplementary to those obtained in the optical examination, should now be evident. Uniaxial crystals can be allocated to their correct systems by a Laue photograph taken with the X-ray beam along the z axis. The Laue photograph in Fig. 5.13 exhibits the Laue symmetry $3m$. Distinction between the monoclinic and orthorhombic systems, which is not always possible in an optical examination, is fairly straightforward with Laue photographs, Table 1.6. Cubic crystals can exhibit a variety of symmetries, but with the X-ray beam along $\langle 100 \rangle$ the differentiation between Laue groups $m\bar{3}$ and $m\bar{3}m$ is clear.

In practice, the symmetry pattern on a Laue photograph is very sensitive to the precise orientation of the crystal with respect to the X-ray beam [5]. Slight deviation from the ideal position will result in a distortion of the relative positions and intensities of the spots on the photographs.

5.4.3 Laue Method and Synchrotron Radiation

The synchrotron is an extremely powerful source of X-rays and produces a very wide range of wavelengths, Sect. 3.1.6, and is ideally suited to the Laue method of recording diffraction patterns. Since the crystal is in a fixed orientation, the angle of incidence of the X-ray beam is thus set for each (hkl) plane. For a reflection to take place at a preset θ angle, the plane must effectively select the wavelength required to satisfy the Bragg equation. A reflection on a Laue photograph thus comprises four parameters, the usual hkl indices and the wavelength selected by the crystal.

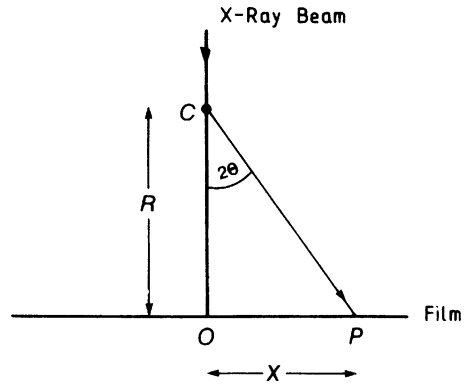

Fig. 5.15 Geometry of Laue diffraction at the level $Y = 0$ on a film placed perpendicularly to the incident X-ray beam: C, crystal; P, position of a Bragg reflection; 2θ, scattering angle

Consider a fixed crystal in a Laue diffraction experiment. For planes (hkl) the preset angle of incidence is θ, and the wavelength required to be selected for the Bragg equation to be satisfied for the reflection hkl is $\lambda(hkl)_\theta$, given by

$$\lambda(hkl)_\theta = 2d(hkl)\ \sin\theta \tag{5.1}$$

For planes $(2h, 2k, 2l)$, the wavelength to be selected is

$$\lambda(2h, 2k, 2l)_\theta = 2d(2h, 2k, 2l)\ \sin\theta \tag{5.2}$$

From Sect. 2.3,

$$\lambda(2h, 2k, 2l)_\theta = 2d(hkl)\ \sin\theta/2 = \lambda(hkl)_\theta/2 \tag{5.3}$$

which is easily generalized to

$$\lambda(nh, nk, nl)_\theta = \lambda(hkl)_\theta/n \tag{5.4}$$

Since the Bragg angle θ is common to the sets of reflections $(hkl, 2h, 2k, 2l, \ldots, nh, nk, nl, n = 1, 2, 3, \ldots)$ these sets will be superimposed on the Laue photograph. The extent of superimposition depends on the range of values of λ available from the X-ray source, which may be selected to minimize this overlap of reflections.

The interpretation of a Laue photograph may thus be complicated both by the possible existence of multiple reflection orders and by the need to assign the correct value of λ to each $I(hkl)$ prior to use in structure analysis. The latter requirement is, of course, necessary in view of the dependence of the atomic scattering factor f on both θ and λ. Other factors requiring special attention include sensitivity characteristics and absorption by the photographic film, both of which are wavelength-dependent.

As an example, consider the following situation: an orthorhombic crystal with $a = 10.0$ Å, $b = 15.0$ Å, $c = 20.0$ Å is mounted with c vertical and perpendicular to the X-ray beam, such that b makes an angle ϕ of 30° with the beam direction in the horizontal plane. A diffraction spot P occurs on a flat-plate film such that its coordinates are X mm (horizontal) and Y mm (vertical), the plate being placed at a distance R mm from the crystal, Fig. 5.15, $Y = 0$. Since the wavelength is variable,

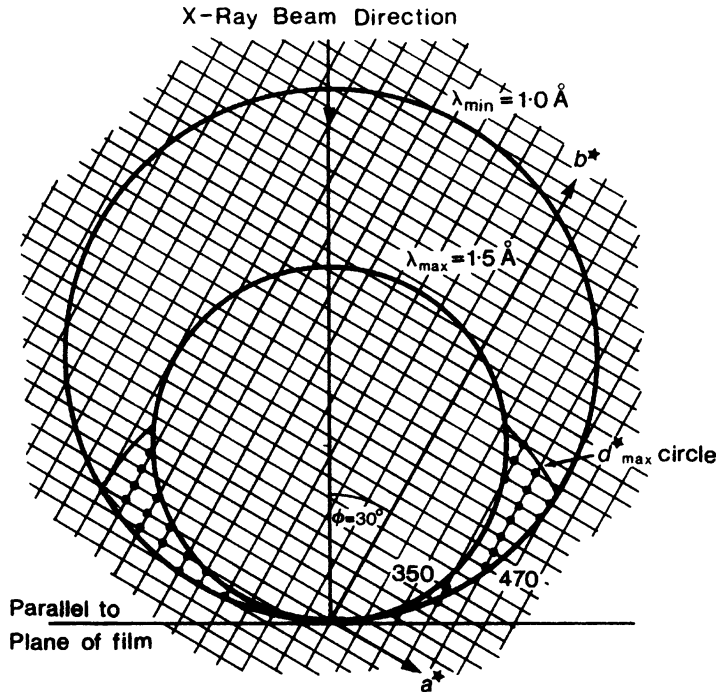

Fig. 5.16 Reciprocal net a^*b^* for an orthorhombic crystal with $a = 10$ Å and $b = 15$ Å, tilted at $\phi = 30°$ to the X-ray beam; c is vertical. The wavelength range chosen is 1.0 Å (λ_{min}) to 1.5 Å (λ_{max}). Reciprocal lattice points that can give rise to diffraction spots on the right-hand side of the film (including the 350 and 470 used in the example calculations) and on the left-hand side have been emphasized. They lie between the limiting arcs of the Ewald spheres as shown. The range of $hk0$ reflections is limited also by the resolution limit d^*_{max}, which is governed by the crystal. For the reciprocal net chosen, $a^* = 1/a = 0.1$ RU and $b^* = 1/b = 0.0667$ RU; the scale is 1 RU = 3.52 cm

we define $d^*(hkl)$ from (2.11) with $\kappa = 1$, which results in the Ewald sphere having a wavelength-dependent radius of $1/\lambda$. Thus, if the extremes of λ used in the experiment are λ_{min} and λ_{max}, the corresponding Ewald spheres will have radii $1/\lambda_{min}$ and $1/\lambda_{max}$, Fig. 5.16. The reciprocal lattice in this treatment has fixed dimensions, $a^* = 1/a$, $b^* = 1/b$, and $c^* = 1/c$. We can predict possible Laue reflections at $Y = 0$ with the aid of Fig. 5.16. The a^*b^* reciprocal lattice net is shown rotated at 30° to the X-ray beam, as described above. Traces of the outer and inner Ewald spheres, corresponding to the minimum and maximum wavelengths, contain a reciprocal lattice area which includes all reciprocal lattice points, shown intensified in the diagram, that are able to give rise to Laue reflections with an appropriate wavelength. The recording geometry relevant to the above experimental arrangement is shown in Fig. 5.15, from which it can be seen that for $Y = 0$ (corresponding to $l = 0$ in the example)

$$\tan 2\theta(hk0) = X/R$$

where X is the horizontal distance of spot P from the origin O, and R is the crystal–film constant. Reciprocal lattice points lying within the allowed region, Fig. 5.16, include 350, 470, 480, 490,..., 313,0, for the limiting wavelengths $\lambda_{min} = 1.0$ Å, $\lambda_{max} = 1.5$ Å used in the example. We now determine the coordinates of Laue diffraction spots and the wavelengths used in producing them.

The wavelength selected for a particular $d^*(hk0)$ can be calculated with reference to Fig. 5.17. In this diagram

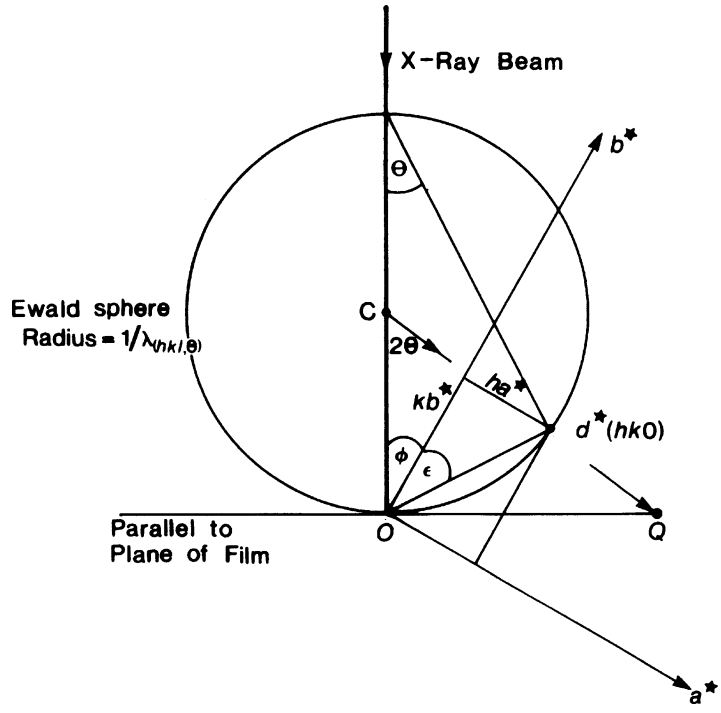

Fig. 5.17 Geometry of wavelength selection through a reciprocal lattice vector d^* ($hk0$). The angle ϕ defines the crystal orientation: C, crystal; O, origin of reciprocal lattice; CQ, direction of diffracted beam

$$\tan\varepsilon = ha* /kb* = hb/ka$$

and

$$\theta(hk0) = [90 - (\phi + \varepsilon)]$$

Thus,

$$\lambda(hk0)_\theta = 2d(hk0)\ \sin\theta(hk0) = 2d(hk0)\ \sin[90 - (\phi + \varepsilon)] = 2d(hk0)\ \cos(\phi + \varepsilon)$$

Taking $\phi = 30°$:

1. Reflection 350

$$\tan\varepsilon = 3 \times 15/(5 \times 10) = 0.900 \qquad \varepsilon = 41.99°$$

$$d(350) = \left(\frac{9}{10^2} + \frac{25}{15^2}\right)^{-1/2} = 2.2299\text{Å} = 2.2299\ \text{A}\therefore\ \lambda(350)_\theta = 2 \times 2.2299\cos(30 + 41.99)$$
$$= 1.3789\ \text{A} \quad \theta(350) = 90 - (30 + 41.99) = 18.01°$$

Hence for $R = 60$ mm

$$X(350) = 60\tan(2 \times 18.01) = 43.62\ mm$$

2. Reflection 470

$$tan\,\varepsilon = 4 \times 15/(7 \times 10) = 0.8571 \qquad \varepsilon = 40.60^\circ$$

$$d(470) = \left(\frac{16}{10^2} + \frac{49}{15^2}\right)^{-1/2} = 1.6270\,\text{Å} \quad \lambda(470)_\theta = 2 \times 1.6270 \cos(30 + 40.60)$$
$$= 1.0809\text{Å} \quad \theta(470) = 90 - (30 + 40.60) = 19.40^\circ \quad X(470) = 60 \tan(2 \times 19.40)$$
$$= 48.24\,mm$$

Note the dependence on these results of the crystal orientation parameter ϕ. It is easy to show that for $\phi = 0^\circ$

1. $\lambda(350)_\theta = 3.3148$ Å
2. $\lambda(470)_\theta = 2.4707$ Å

Thus, neither of these reflections would be recorded for this orientation using the given wavelength range.

Laue photographs can be scanned optically with a densitometer, which records both intensity and position of each spot on the film; alternatively, this information can be derived from the diffraction pattern recorded on a flat reusable CCD plate. These data are then processed by computer using powerful software, which will index and also refine the unit-cell parameters as required, Sect. 11.2.3ff.

The interpretation of such records, which can contain thousands of spots, is a skilled operation but usually requires a minimum of user intervention. Knowledge of the crystal unit cell is a useful prerequisite; otherwise the crystal can be, and usually is, randomly oriented with respect to the direction of the X-ray beam. With a crystal of high symmetry it is possible to record most of the three-dimensional diffraction pattern on a single photograph. Being independent of mechanical constraints, Laue data can be recorded very rapidly, in seconds for good quality crystals at a high-intensity synchrotron radiation facility using a CCD plate (q.v.) instead of a photographic film. Even the problem previously mentioned of multiplicity of orders has proved to be less of a difficulty to an application of the method than at first thought, for example, by using a wavelength range of 0.6–1.6 Å in protein crystallography.

The method thus facilitates novel studies using synchrotron radiation, such as time-dependent solid-state reactions and enzyme-driven transformations. The latter can be synchronized by employing tailor-made photosensitive substrates to delay the biochemical reactions until the X-ray experiment is ready. Such studies provide exciting new dimensions to X-ray crystallography.

There are several important differences between synchrotron radiation and X-rays generated from a conventional laboratory source. The latter are usually emitted as characteristic radiation from a copper or molybdenum metal target, and comprise the predominant characteristic α and β wavelengths, and a more general, less intense, polychromatic background. An appropriately selected metal filter allows the production an effectively monochromatic beam, Sect. 3.1.4. Synchrotron radiation (SR) is of extremely high intensity, a property which can be exploited for the examination of weakly diffracting or very small crystals. A particular wavelength can be selected from the continuous SR wavelength range by an appropriate filter, for either single-crystal rotation or powder diffraction experiments. Alternatively, the continuous polychromatic beam can be used for Laue photography with a stationary crystal, to record diffraction data efficiently and rapidly. Finally, SR has a very low beam divergence which results in very sharp diffraction spots, Fig. 5.18. This is particularly useful in providing good intensity data from poorly diffracting crystals, such as proteins, resulting subsequently in greatly improved resolution of their X-ray Fourier images.

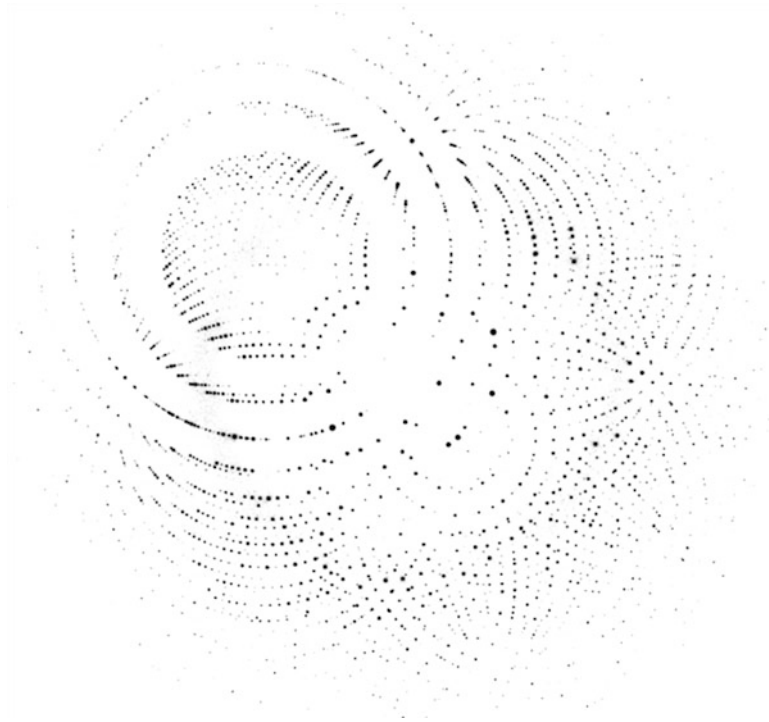

Fig. 5.18 Synchrotron Laue photograph recorded from a crystal of Photoactive Yellow Protein (PYP) recorded on the ESRF Laue beam line (ID09B). The exposure was performed by accumulating 16 single pulses each 100 ps long (courtesy H. Ihee and M. Wulff, ESRF, Grenoble)

5.4.4 Oscillation Method

Flat-Plate Oscillation Technique: Basic Ideas

This technique is now used for both preliminary assessment of the suitability of a crystal prior to X-ray data collection and data collection itself with monochromatic X-radiation. The diffraction pattern was originally recorded on a flat film, but has been replaced in modern applications by one of several electronic devices known as area detectors or position-sensitive devices that we discuss in Sect. 5.7.

The intensity data are recorded in a series of exposures in which the crystal is rotated or oscillated through a small angular range $\delta\varphi$ of about 0.1–2°. For crystals with large unit cells, it is necessary to employ a large crystal–film distance, at least 60 mm, in order to effect separation of the diffraction spots on the film. A large effective surface area is necessary in order to record data to high resolution, that is, to high θ values, for the production of good quality X-ray structure determinations. Previously, cameras were designed specifically for this purpose, and employed a flat-plate film perpendicular to the X-ray beam together with a mechanism for automatically changing the cassette, a carousel device, thus enabling several exposures to be set concurrently [6]. Area detectors, Sect. 5.7, are reusable, thus eliminating this requirement.

The geometry necessary to define the (X, Y) coordinates of an upper-level spot on the film or plate is indicated in Fig. 5.19. In this diagram CO' is perpendicular to the film plane. Triangle $CO'P'$ is right-angled at O', and $PP'O'$ at P'; triangles $DD'C$ and $PP'C$ are similar, so that

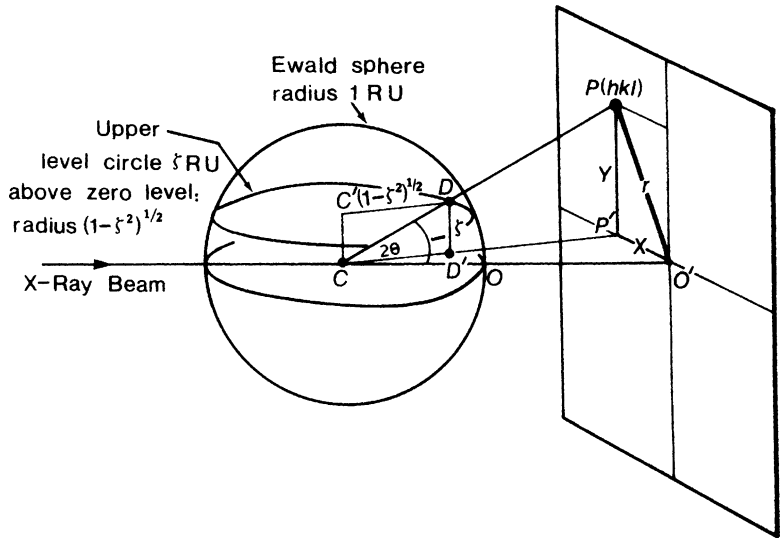

Fig. 5.19 Coordinate pair X, Y of the diffraction spot P on a flat-plate oscillation photograph for a general upper-level reflection: C, crystal; CC', oscillation, or φ axis; O, reciprocal lattice origin; O', origin of coordinates on the film; $OD = d^*(hkl)$; CP, reflected beam, intersecting the Ewald sphere at D; DD', perpendicular distance above the zero level. Since the radius of the Ewald sphere is 1 RU, the radius of the upper level at level ζ is $\sqrt{(1-\zeta^2)}$; CO' is the crystal-to-film distance

$$\begin{aligned} Y/CP' &= \zeta/CD' = \zeta/(1-\zeta^2)^{1/2} \\ Y &= CP'\zeta/(1-\zeta^2)^{1/2} \\ CP'^2 &= R^2 + X^2 \\ Y^2 &= (R^2 + X^2)\zeta/(1-\zeta^2) \end{aligned} \tag{5.5}$$

where R is the distance CO'.

Further,

$$r/R = \tan 2\theta \quad \text{and} \quad r^2 = X^2 + Y^2$$

where r is the distance PO'. Therefore,

$$R^2\tan^2 2\theta = X^2 + Y^2 \tag{5.6}$$

Combining these results, it follows that

$$X = R[\tan^2 2\theta(1-\zeta^2) - \zeta^2]^{1/2} \tag{5.7}$$

$$Y = R\zeta[1 + \tan^2 2\theta]^{1/2} \tag{5.8}$$

If a reciprocal lattice axis is parallel to the rotation axis, ζ RU corresponds to the appropriate level along the axis.

We will illustrate these ideas with the following worked example. A protein crystal with a monoclinic unit cell, $a = 30.0$ Å, $b = 50.0$ Å, $c = 40.0$ Å, $\beta = 100°$, is mounted on an oscillation camera equipped with a flat-plate cassette placed with its plane perpendicular to the X-ray beam and at a distance $R = 60$ mm from the center of oscillation. The b axis of the crystal is vertical and perpendicular to the X-ray beam, with $-a$ parallel to the beam at the start of a counterclockwise rotation; X-rays with wavelength of 1.2 Å are used in the experiment. Consider the following problems:

1. At what point in the rotation will the 004 reflection take place?
2. Calculate the (X, Y) coordinates (in mm) of the 004 spot on the film, X being the horizontal coordinate and Y the vertical.
3. Calculate the (X,Y) coordinates (in mm) of the 014 spot on the film.

1. Refer to Fig. 5.18 to see that the required rotation is $\theta(004)$, calculated as follows:

$$d^*(004) = 4c^*$$

where $c^* = \lambda/c \sin\beta = 1.2/(40 \sin 100) = 0.03046$, so that

$$d^*(004) = 0.1219 = 2 \sin\theta(004)$$

Hence, $\sin\theta(004) = 0.06095$ and $\theta(004) = 3.494°$ (the rotation angle from starting position).

2. From Fig. 5.20, we have

$$\begin{aligned} X(004) &= R \tan 2\theta(004) \\ &= 60 \tan 6.988 \\ &= 7.354 \text{ mm} \\ Y(004) &= 0 \text{ mm} \end{aligned}$$

3. For the 014 reflection:

$$\zeta = b^* = \lambda/b = 0.0240$$

Using (2.16), it follows that

$$\begin{aligned} d^{*2}(014) &= b^{*2} + 16c^{*2} \\ &= 0.0240^2 + 16(0.03046)^2 \\ &= 0.01542 \end{aligned}$$

so that

$$d^*(014) = 0.1242 = 2 \sin\theta(014)$$

Hence, $\sin\theta(014) = 0.06210$, and $2\theta = 7.121°$, by (5.7). Thus,

$$X(014) = 60[\tan^2 7.121(1 - 0.0240^2) - 0.0240^2]^{1/2} = 7.352\, mm$$

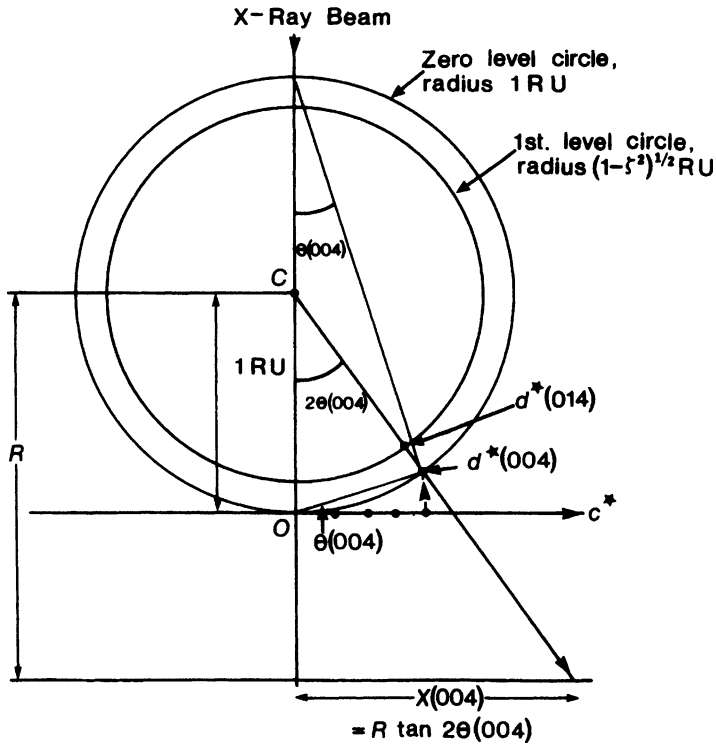

Fig. 5.20 Plan view of flat-plate oscillation geometry, looking down the oscillation axis, CC' in Fig. 5.19, at C. In the accompanying example, the y axis of the crystal (C) is perpendicular to the diagram, and coincides with the rotation axis. Because the crystal is monoclinic, the a^*c^* levels superimpose in this orientation. The diagram shows c^* at the beginning of an anticlockwise rotation perpendicular to the X-ray beam. The crystal rotates through $\theta(004)$ and, at the reciprocal lattice point 004, d^* (004) intersects the Ewald sphere and the 004 reflection is produced. For the 014 reflection, a further small rotation is necessary

and from (5.8)

$$Y(014) = 60 \times 0.0240[1 + \tan^2 7.121]^{1/2} = 1.451 \text{ mm}$$

Hence, the 004 reflection has coordinates (7.354, 0.0) mm; the 014, (7.352, 1.451) mm.

5.5 Measurement of the Intensities of Diffraction Data

A variety of options is open to the crystallographer for obtaining measurements of X-ray intensities. These include the use of a single counter or serial diffractometer, and the latest area detectors. A list of some of the currently available equipment is to be found in Sect. 5.7.10. Examples include the computer-controlled four-circle serial diffractometer (Nonius CAD4), and the kappa geometry CCD diffractometer (Nonius KappaCCD). A cryostream device may be attached for work at low temperatures.

5.5.1 Single Counter or Serial Diffractometers

Traditional diffractometers that employ scintillation counters[1] to detect and measure X-ray reflections from single crystals, one by one, incorporate a mechanical goniometer to orientate the crystal into the correct reflecting position for each *hkl* reflection, and to rotate the counter to receive the scattered radiation from this single reflection. The energy is transformed electronically into a form suitable for conversion to $I(hkl)$. Because each reflection is measured individually, with a count time typically of around 60 s, the process is very slow, particularly for proteins, which routinely involve the measurement of tens of thousands of reflections. The dynamic range of the instrument is the quantified range of intensities from very weak to very strong over which the instrument can produce measured values of intensity. This can be enhanced to enable measurement of very strong reflections through the use of a calibrated attenuator, such as a strip of nickel foil in the case of copper radiation. The wider the dynamic range available the better will be the measured set of intensity data. For relatively unstable crystals, proteins and other macromolecules, the crystal needs to be replaced once it is observed to be dying. Consequently, several crystals may be required in the production of a complete data set, which is subsequently achieved by scaling the individual sets together. However, the accuracy attainable is possibly better than for most other methods, and this advantage offsets the lengthy time scale that is required for the data collection.

The disadvantages of a slow data-collection rate and the need for several crystals with single counter diffractometry have been largely overcome by the use of electronic film *area detectors* and *image plates*, which methods we discuss in Sect. 5.7.

5.6 Single-Crystal X-Ray Diffractometry

It has become commonplace for X-ray diffraction data to be collected by means of a diffractometer. We give here a brief description of the Enraf–Nonius CAD4 kappa-diffractometer. Two other similar systems are considered later.

5.6.1 Instrument Geometry

The CAD4 kappa-diffractometer is characterized by its κ-goniometer, which differs in geometry from other four-circle diffractometers. The κ-goniometer carries the goniometer head and arcs, and keeps the crystal at the center of the diffractometer throughout the data collection. The κ-goniometer is a combination of three parts, which carry the rotation axes. All axes intersect in the center of the diffractometer.

The arcs are mounted on the ϕ axis, on the κ-block, as shown in Fig. 5.21; the angle of rotation about this axis is ϕ_κ. The κ-block is rotated about the κ axis, being itself carried by the ω-block. In turn, the ω-block is rotated about the axis (ω_κ) and is carried on the diffractometer base. The angle χ between the ω and X axes is ca. 50°, and that between the κ and ϕ axes is also ca. 50°. Thus, the goniometer can access all directions of χ within about 100° of the zero setting of the instrument. This suspension gives the CAD4 an enhanced flexibility over the traditional Eulerian cradle. There is also a 2θ axis, coinciding with the ω axis, which carries the scintillation counter detector. The coincidence of the ϕ and ω axes corresponds to $\kappa = 0$; $\omega_\kappa = 0$ for κ in the plane of the diffractometer axes X and

[1] Similar to Geiger counters.

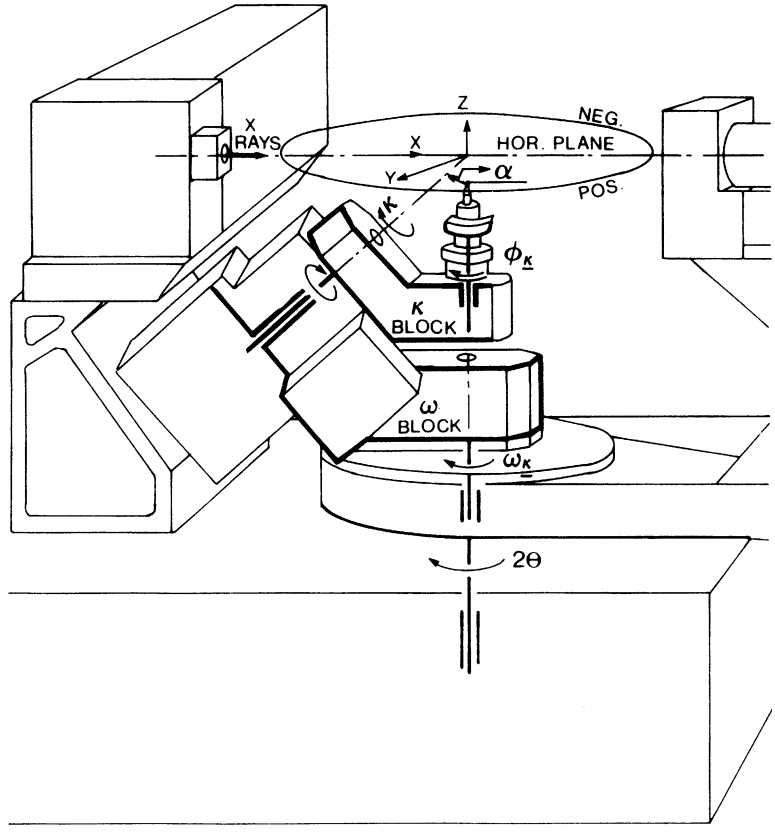

Fig. 5.21 Schematic diagram of the Nonius CAD4 single crystal X-ray κ diffractometer, showing the X, Y, Z instrumental coordinate system and the rotation directions (reproduced with the permission of Enraf–Nonius, Delft)

Z, with the κ block opposite $+X$, and $2\theta = 0$ when the center of the detector lies in the plane of X and Z and opposite $+X$. The definition of ϕ_κ is arbitrary, and a suitable working procedure is arranged. Starting from $\kappa = \omega_\kappa = 0$, positive rotations of θ, ω, and ϕ move a vector from Y toward X, and a positive rotation about κ moves a vector from Y to a position below the horizontal plane.

5.6.2 Rotation of the Crystal into a Diffracting Position

In the zero position of the CAD4, a vector **c** is assumed to be attached to the crystal, with components c_1, c_2, and c_3 parallel to X, Y, and Z, respectively. The operation to be applied to **c** is given in terms of the angles ω_κ, κ, ϕ_κ by

$$c(\omega, \kappa, \phi) = Z(\omega_\kappa) \cdot Y(-\alpha) \cdot Z(\kappa) \cdot Y(\alpha) \cdot Z(\phi_\kappa) \cdot |c| \tag{5.9}$$

We can define general clockwise rotations of amounts α, β, and γ about X, Y, and Z, respectively, by the following matrices:

$$X(\alpha)_{Z \to Y} = \begin{bmatrix} 1 & 0 & 0 \\ 0 & \cos\alpha & \sin\alpha \\ 0 & -\sin\alpha & \cos\alpha \end{bmatrix} \tag{5.10}$$

$$Y(\beta)_{X\to Z} = \begin{bmatrix} \cos\beta & 0 & -\sin\beta \\ 0 & 1 & 0 \\ \sin\beta & 0 & \cos\beta \end{bmatrix} \tag{5.11}$$

$$Z(\gamma)_{Y\to X} = \begin{bmatrix} \cos\gamma & \sin\gamma & 0 \\ -\sin\gamma & \cos\gamma & 0 \\ 0 & 0 & 1 \end{bmatrix} \tag{5.12}$$

In (5.9), α is the angle of rotation of the κ-block about Y such that the κ and Z axes coincide. The term $Y(-\alpha)$ in (5.9) returns the goniometer to its original position.

5.6.3 Transformation from Miller Indices to Diffractometer Angles

To set a reflecting plane in the diffracting position, its Miller indices are transformed to a scattering vector **c** by an orientation matrix **R**:

$$\mathbf{R} = \begin{bmatrix} a_X^* & b_X^* & c_X^* \\ a_Y^* & b_Y^* & c_Y^* \\ a_Z^* & b_Z^* & c_Z^* \end{bmatrix} \tag{5.13}$$

where the reciprocal unit-cell vectors $\mathbf{a}^*$, $\mathbf{b}^*$, and $\mathbf{c}^*$ are resolved into components along X, Y, and Z respectively. Then

$$\begin{bmatrix} c_1 \\ c_2 \\ c_3 \end{bmatrix} = \mathbf{R} \cdot \begin{bmatrix} h \\ k \\ l \end{bmatrix} \tag{5.14}$$

or

$$c = \mathbf{R} \cdot h \tag{5.15}$$

Other similar transformations are built into the software of the diffractometer so that the scattering vector **c** is brought into the horizontal plane and, via Eulerian forward and inverse transformations, for mathematical convenience, the values of the angles ω_κ, κ, and ϕ_κ, by which the diffractometer circles must be moved, are determined. Then the intensity of the reflection that corresponds to $\mathbf{c}(\omega_\kappa, \kappa, \phi_\kappa)$ can be measured and recorded.

5.6.4 Data Collection

The flexible routines that are built into the CAD4 permit selection of the *hkl* reflection in differing ways, including Friedel pairs *hkl* and $\bar{h}\,\bar{k}\,\bar{l}$, Sects. 3.6.1 and 7.5. The azimuthal angle, the angle between the vertical and the normal to the ϕ-circle, can be variously specified, including multiple measurements of reflections at different azimuth values so as to derive an empirical absorption correction curve as a function of the angle ϕ, see Sect. 4.1.3.

Intensity and background measurements are carried out, and the crystal may be monitored for decay and movement. Where the latter occurs, the crystal may be reoriented as necessary during the data collection. If the space group is known, only the geometrically permitted reflections need to be scanned. This procedure is of great significance with centered unit cells. In addition, more than the unique portion of reciprocal space can be explored. By means of the CAD4 Structure Determination Package, the symmetry-equivalent reflections can be merged to give the best set of unique data, Lorentz and polarization corrections applied, and an absorption correction included if deemed desirable. The data set can be truncated so as to exclude weak reflections of lower accuracy, for example, those for which F_o^2 is less than $3\sigma(F_o^2)$, or they may be remeasured over a longer time period so as to increase their precision. The CAD4 is provided with a means of taking X-ray photographs of the crystal on the diffractometer, using Polaroid film. This procedure may be very helpful where there is a "difficult" space group, or where twinning is suspected, but it may not prove a substitute for a thorough initial examination of the crystal by conventional X-ray photography where necessary.

The automatic search and indexing routines for determining the unit cell are not always definitive. This situation may arise for various reasons, such as twinning, poor crystal quality, leading to weak reflections, or insufficient spread of reflections in reciprocal space. Several options are available for operator intervention. One of the most useful is to take a Polaroid rotation photograph about the randomly oriented ϕ-axis and use it to determine the x, y coordinates of reflections on the film. About ten such pairs of values will often suffice to determine an approximate unit cell. Then the unit cell can be refined by locating more reflections, well distributed in reciprocal space, and applying a least-squares procedure, Sect. 8.4.2. The ϕ-axis photograph may detect poor crystal quality but not twinning, and it will not help with space-group determination; normal rotation X-ray photographs about the crystallographic axes may be helpful in these situations, but this procedure is rarely used nowadays.

The techniques available with the CAD4 have been well tested in laboratories throughout the world, and their careful application can lead to a data set of high quality, capable of solving and refining a crystal structure to high precision, with R-factor (q.v.) between 5 and 1%.

5.6.5 Scanning Over a Peak: ω/θ Versus ω Scans

The most widely used, and arguably the best, scanning option employed with the CAD4 and similar types of diffractometer involves a coupled rotation of the crystal (ω-axis) and the counter (2θ-axis), Fig. 5.21, both rotation axes being vertical during the scan. For a given reflection, the center of the scan coincides with the calculated position of the maximum intensity, based on the orientation matrix and unit-cell parameters already determined. Figure 5.22 shows the variation of intensity recorded for such a scan, using a good quality crystal. In order to obtain a measure of the intensity it is necessary to evaluate the counts recorded in the area P on the diagram. For most reflections there is general background intensity, shown in the diagram as being slightly asymmetrical. The background levels $B1$ and $B2$ are established by short scans on either side of the peak.

The scans are not smooth, and consist of, say, n short steps in both $B1$ and $B2$ and m similar steps in P. If the total counts are $b1$ for region $B1$, $b2$ for region $B2$, and N for the peak P, it can be shown that the number of counts in P is $[N - m(b1 + b2)/2n]$. For most small-molecule crystals, the peak width would be about 40–60 min of arc and the total scan time about 60 s. In this method the two backgrounds are usually fairly similar. The facility for inspecting individual scans is extremely useful for establishing the correct scan width to use for a given crystal, and to check for crystal splitting, which would produce a double, or even a multiple, peak.

For crystals with very large unit cells, which occur mainly with macromolecules, neighboring peaks are usually too close together, because the reciprocal lattice constants are very small, to allow the use

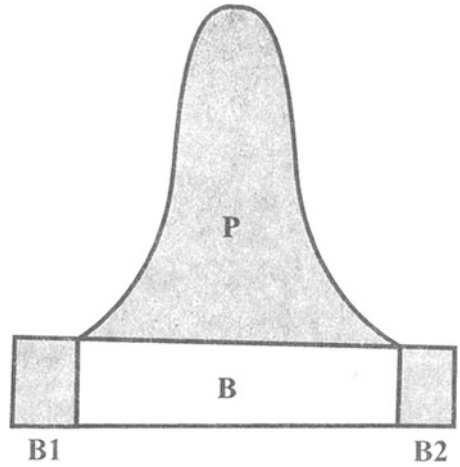

Fig. 5.22 Profile of a reflection peak scanned in the ω/θ mode. The background level to be subtracted on either side of the peak is indicated. It is typically slightly asymmetrical

of ω/θ scans. Instead, the alternative ω-scan method is used, which involves a stationary counter, fixed at the correct value of 2θ. This procedure reduces the possibility of the diffraction maxima for neighboring reflections overlapping, but does not eliminate it altogether.

5.7 Area Detectors (Position-Sensitive Detectors)

The disadvantages of single counter diffractometry, mentioned earlier, that apply mainly to large-molecule structures, are a slow data-collection rate and the requirement of several crystals for collection of a complete data set, with the attendant errors associated with scaling and crystal deterioration: macromolecular crystals may contain 40–50% of solvent, which renders them susceptible to decay in the X-ray beam. These problems have been largely overcome by the use of electronic film *area detectors* and *image plates* that have enjoyed rapid development in recent years. In many laboratories, these methods of detection are used for both large- and small-molecule crystallography, and especially in structure determination at low temperature.

The use of an *area detector* or *image plate* allows many nonoverlapping reflections to be recorded in a single exposure. Each exposure is produced by oscillating the crystal through a small angle, $\Delta\varphi$. Each reflection is received by a detector, which is an effectively flat surface with a uniform sensitivity to X-rays. A series of sequential exposures is recorded, during which the crystal may be rotated through a total of 180°, for a triclinic crystal, or as little as 30°, for a hexagonal or cubic crystal. The X, Y position of each reflection (Fig. 5.19) enables its hkl index to be computed, and the signals received at the detector are converted electronically into intensity data. Area detectors are therefore also position-sensitive detectors, because both the intensity of a diffracted beam and the exact position where it strikes the detector are determined. Several designs are commercially available, as discussed next.

5.7.1 Multiwire Proportional Counter

The multiwire proportional counter (MWPC) is a digital detector, working on the principle of detection of X-rays by ionization. This type of detector was used by protein crystallographers in

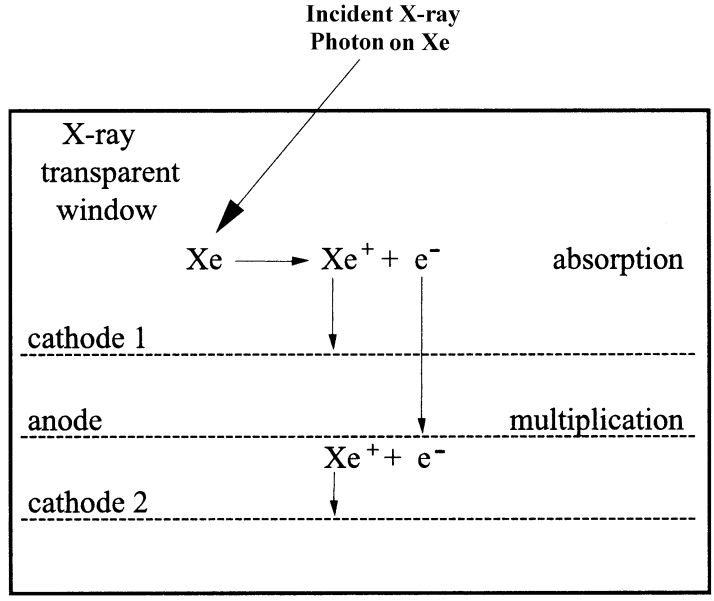

Fig. 5.23 Principle of the multiwire proportional counter (MWPC)

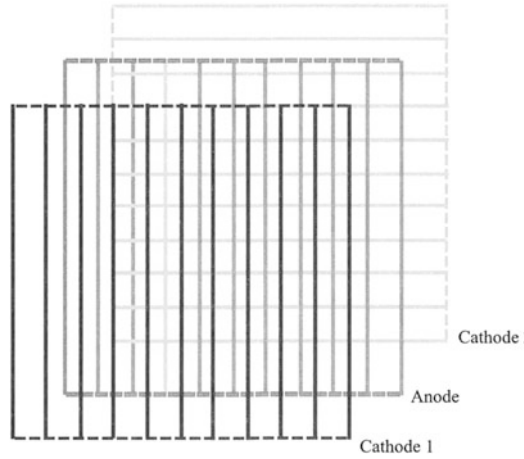

Fig. 5.24 Design of the MWPC

the 1980s and 1990s. The design of the MWPC is based on a xenon-filled chamber with an anode lying between two cathodes, Fig. 5.23. Each anode and each cathode consists of a plane of parallel wires, with the direction of the wires in the first cathode and the anode perpendicular to those in the second cathode, Fig. 5.24. During exposure to X-radiation, X-ray photons enter the chamber. For each photon that is absorbed, a xenon molecule is ionized into a positive xenon ion and an inner shell electron having a kinetic energy that is virtually all of the energy of the absorbed photon. The liberated electron ionizes further xenon molecules. In the case of Cu $K\alpha$ radiation, a single 8 keV photon, the energy of a Cu $K\alpha$ photon, produces about 300 ions and primary electrons. An electric

field accelerates the positive ions toward the first cathode and the cloud of electrons toward the anode. The electron cloud passes the first cathode to hit the anode plane, producing an avalanche of secondary ionization, with an amplification factor of the order of 10^4 or more for each primary electron. While the electrons give a negative pulse on the nearest anode wire, the positive ions move toward the second cathode giving a positive pulse on the nearest cathode wire. To prevent ultraviolet photons, produced in the secondary ionization, from restarting ionization in another region of the chamber, a small amount of quenching gas, such as methane, is added to the xenon and absorbs excess photons and dissipates energy. Counting is accomplished through the orthogonal array of wires that samples the centroid of the charge distribution. The analog signals from the detector are digitized to produce the corresponding reading.

This type of counter has a low noise level, is extremely sensitive, and covers a wide dynamic range of intensities. Unfortunately the MWPC is severely hampered by size limitations, which reduce the resolution range achievable with Cu $K\alpha$ radiation, suffer from errors due to parallax at high angles of incidence, and require a helium path in order to limit absorption, because of the large crystal-to-detector distances employed. Commercially available MWPC devices include the Bruker AXS HI-STAR (11.5 cm diameter) and the larger Xuong–Hamlin (also called San Diego Multiwire System or SDMS, 30 $\times$ 30 cm).

5.7.2 FAST Area Detector (Enraf–Nonius FAST) [3]

In this method, the X-ray reflections strike a phosphor coated fiber optics screen that converts the signals into light photons, which are then intensified, integrated, and digitized. The recording device incorporates a television scanning system and the goniometer is essentially that used in the CAD4 diffractometer. The disadvantages of this method include high electronic noise and consequent low dynamic range ($1{:}10^3$) and the need for remeasurement of strong intensities at decreased camera voltage. In view of these inherent difficulties the FAST technique is now seldom used.

5.7.3 Image Plate

The image-plate detector [7, 8], shown diagrammatically in Fig. 5.25a, consists of a barium halide phosphor doped with divalent europium, BaFBrEu(II), and held in an organic binder. On exposure to X-rays, an X-ray photon hits the image plate and its energy is stored in a Br^- "hole" (an F-center defect) and the Eu(II) species is excited into the metastable Eu(III) state until further stimulated:

$$\mathrm{Eu(II)} \xrightarrow{\text{X-rays}} \mathrm{Eu(III)} + \mathrm{e}$$

(see also Fig. 5.25b). After completion of each exposure, during which time the crystal is oscillated in the X-ray beam for a few minutes, the image plate is scanned with a narrow {helium– neon laser beam (Fig. 5.25c), which causes the regions converted to Eu(III), where the X-ray spots would be located on a photographic film, to emit violet light of wavelength 3900Å with intensity proportional to the absorbed X-ray energy.

$$\mathrm{Eu(III)} + \mathrm{e} \xrightarrow{\text{laser}} \mathrm{Eu(II)} + \mathrm{h}\nu\ (\text{blue - violet})$$

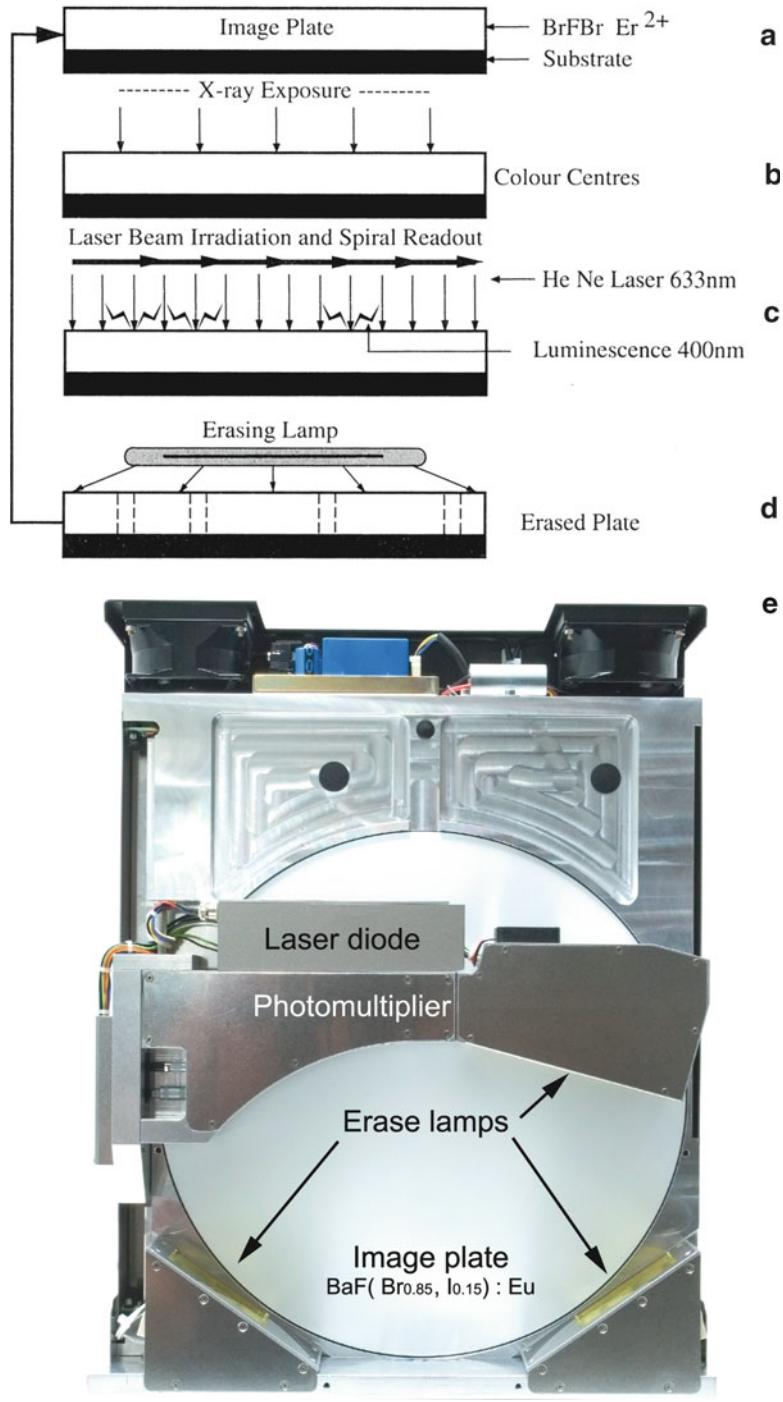

Fig. 5.25 (**a**) Resting state of the image plate. (**b**) Exposure to X-ray diffraction from the oscillating crystal. (**c**) Scanning with laser light and measurement of the emitted light from each spot with a photomultiplier. (**d**) Cleaning the plate ready for further use (**e**) Front view of MAR 345 image plate

This light is then detected with a photomultiplier system, integrated and digitized. After reading the stored data, the plate is cleaned by exposure to bright yellow light, Fig. 5.25d, and it is then ready to record the next image. Image plates up to 345 mm diameter are now available (Mar Image Plate 345), which enable data to be collected to a resolution of about 1.4 Å using Cu $K\alpha$ radiation, and even

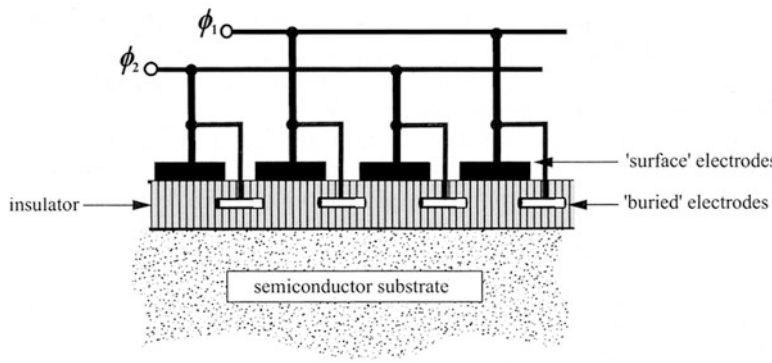

Fig. 5.26 Design of a CCD chip

better resolution with synchrotron radiation at smaller radiation wavelengths. The resolution restriction normally precludes the choice of this device for routine small-molecule analysis, but it is very popular for large-molecule work. An approximately $1{:}10^5$ range of intensities can be recorded compared with ca. 1:200 for X-ray film.

5.7.4 Charge-Coupled Device Area Detectors

In this type of system, which is rapidly becoming the method of choice in both small-molecule and macromolecular crystallography, the video tube of the now almost obsolete FAST area detector, Sect. 5.7.2, or alternatively the image plate, Sect. 5.7.3, is replaced by a charge-coupled device (CCD). The CCD has been developed for a multitude of applications where extremely efficient detection of photons is required, as in astronomy and other branches of physics as well as X-ray crystallography. We could say that the ideal characteristics of a detector are:

- 100% quantum efficiency (independent of wavelength)
- Perfectly uniform response and unlimited dynamic range (both energy-wise)
- Electronically noiseless
- Completely characterized components

Since the conception [9] of the CCD in 1970, the current state of the art has now effectively achieved all of these criteria and the design of the CCD will probably not be improved further. In theory, a CCD performs the following tasks:

1. Generation of charge. When a photon strikes a CCD, it generates electron–hole pairs by the photoelectric effect [10].
2. Collection of the resulting charge or charges in the pixels formed by an array of electrodes or gates.
3. Transference of the charge on each pixel by application of a differential voltage across the gates. This information is conveyed pixel by pixel for counting.
4. Detection of the individual charges and conversion to an output voltage, followed by digital encoding prior to computer processing [11, 12]. Figure 5.26 shows a possible design for a CCD chip.

The detector used with the Nonius Kappa CCD diffractometer, Fig. 5.27, achieves high efficiency through the use of a special grade phosphor (Gd_2O_2S) with directly bonded high-quality fiber optics, in turn also directly bonded to the CCD chip. The CCD chip needs to be actively cooled to between −20 and −50°C, which is achieved through the incorporation of a stack of four Peltier elements again bonded directly to the chip. This results in a stable low temperature at the chip, which is a requirement for low noise and consequent high sensitivity with low background. Figure 5.28 shows a composite

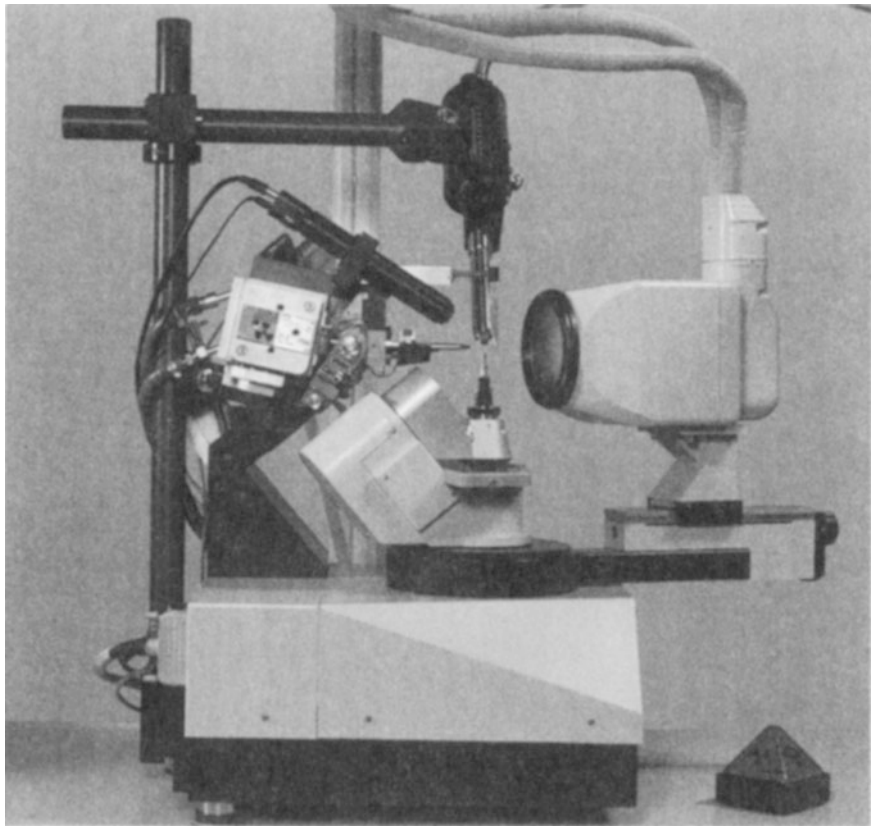

Fig. 5.27 A view of the Nonius Kappa CCD diffractometer

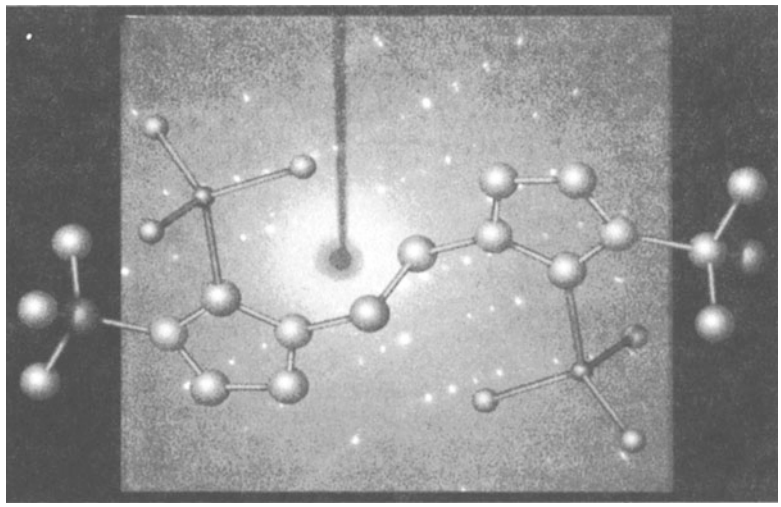

Fig. 5.28 Composite of the molecule 1,2-ethene-3,3′-di-*tert*-butyl-diimidazole-2,2′-diylidene indium(III) trihydride, $C_{16}H_{32}In_2N_4$, superimposed on part of its diffraction pattern, as recorded on a Nonius Kappa CCD diffractometer

representation of the novel molecule 1,2-ethene-3,3′-di-*tert*-butyl-diimidazole-2,2′-diylidene indium (III) trihydride, $C_{16}H_{32}In_2N_4$, superimposed on part of its diffraction pattern, which was recorded on a Nonius Kappa CCD diffractometer [13].

5.7.5 The Tiled CCD

The MAR (Rayonix USA) company has recently introduced the MX-series of detectors described as the tiled continuous CCD which uses either a 3 × 3 or a 4 × 4 array of fiber optic elements so as to make a larger active surface. This is achieved by coupling the detector to a fiber optic, and linking multiple CCD units together.

5.7.6 Charge-Coupled Device Including Tiled CCD Versus Image Plate

Image-plate detectors may be considered to be the heart of the workforce in many of the current applications in recording and digitizing X-ray diffraction data. They have a large active surface, good spatial resolution, and are relatively easy on the financial budget, which is a key consideration in many science departments. Their main drawback has been that the readout time of 60 s is relatively slow. However, recent design improvements, such as the MAR 345 IP, have resulted in a significant reduction of this time to as low as 26 s and can record high-quality data from both small-molecule and macromolecular crystals. The readout time is still slow compared to 1 s or less for a CCD which can record atomic resolution data for small proteins at the synchrotron [13, 14]. In a local laboratory environment this is a minor consideration, because the limited power of the X-ray source means that exposure times of 5–10 min are the norm. At modern synchrotron stations, where beam time is at an absolute premium, IP detectors while being extremely reliable are far too slow. The CCD detector on the other hand is very fast (30–90 s exposures) and the small active surface problems which restrict the range of data collection have now been alleviated by the introduction of the tiled CCD, described in the previous section.

With their high sensitivity, high resolution, and low noise, the CCD is now in regular use for high-resolution macromolecular structure determinations [14, 15]. Diffractometers employing CCD, including software packages, are available from Nonius [16], Bruker [17], and Oxford-diffraction [18], a system which includes optional liquid nitrogen or liquid helium cooling of the crystal (Fig. 5.29a); other systems are run routinely with liquid nitrogen cooling. Figure 5.29b shows a close-up of the Oxford Cryosystems CCD detector.

5.7.7 Data Collection Strategies

X-ray intensity data are measured most frequently using the oscillation technique as described in Sect. 5.4.4, or with one or two minor variations. The crystal may be flash frozen and immediately held in the X-ray beam on a goniometer head for data collection. In-house X-rays are generated using a rotating anode or other high output X-ray tube, Sect. 3.1. For small-molecule analysis a molybdenum X-ray tube may be used and for proteins an X-ray tube with a copper target is chosen; most protein crystals would not give a high-quality data set with molybdenum X-radiation. A highly intense synchrotron source with a wavelength range of 0.7–1.0 Å would be ideal in most cases.

The crystal can be rotated or oscillated about the ϕ axis of the equipment by a preselected amount. Most crystals will arrive on the goniometer head in a random orientation unless care has been taken to

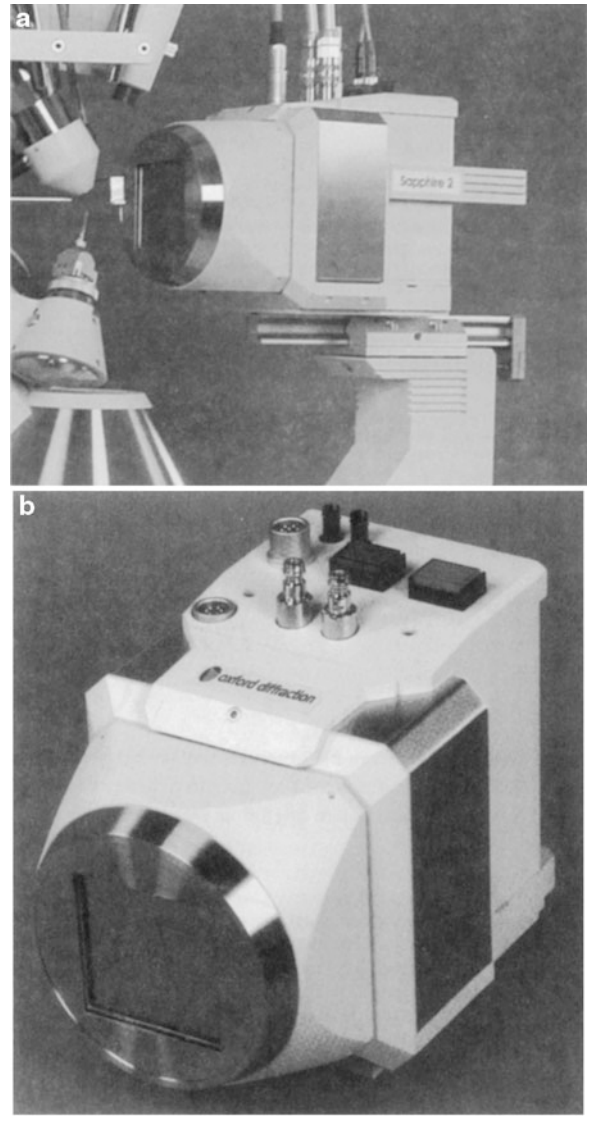

Fig. 5.29 Oxford-diffraction: (**a**) The CCD detector in position at the Oxford-diffraction Xcalibur diffractometer. (**b**) A close-up of the Oxford-diffraction CCD detector (reproduced by permission of Agilent, formerly Oxford Diffraction)

ensure that a particular crystallographic axis is parallel to the ϕ axis. With an IP or CCD detector, data are collected in a series of small angle oscillations of $\Delta\phi$ where $\Delta\phi$ would be selected between 0.1 and 2.0°. The overall angular range of ϕ for the whole data could be 180 or 360° in order to ensure collection of Friedel equivalent reflections. The final data set would then include sufficient measurements to enable the unit cell, space group and R_{int} to be evaluated. It is often possible, and advisable, to derive the unit cell and space group by indexing a subset of the data at an earlier stage in the collection process in order to enable any problems that may emerge to be dealt with. Most software packages will allow an efficient data collection strategy to be designed in order to minimize problems such as radiation damage. Highly intense X-ray sources available at the present time often produce data images that are sufficiently intense to record after a single pass of the crystal through the angular range $\Delta\phi$.

The method of data collection may be designated as *fine-ϕ-slicing* if $\Delta\phi$ is less than or equal to half the reflection, or rocking, width, which is a function of the crystal mosaic spread and beam divergence usually in the range 0.1–1°, or *thick-ϕ-slicing* if $\Delta\phi$ is greater than half the reflection width. At a

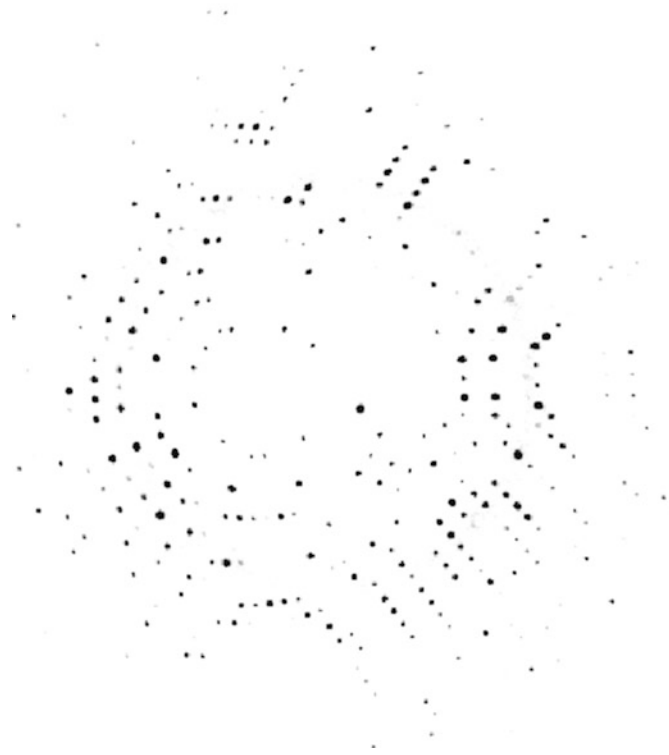

Fig. 5.30 A high-quality oscillation photograph of cryo-cooled cubic insulin recorded using a Bruker Microstar rotating anode source with a Proteum X8 CCD plate; Cu $K\alpha$ X-radiation was used, with crystal-to-detector distance of 45 mm, and a 0.5° oscillation. The image display software was COSMO/SAINT (reproduced by courtesy of Dr. S. M. Prince and Dr. P. K. Bryant, Faculty of Life Sciences, Manchester)

synchrotron source, where the beam divergence is extremely small, a data set with images, or frames, of 1.5° rotation would be a thick data set if the crystal mosaicity was 0.75° but would be a thin or fine data set if the crystal mosaicity was 0.5°.

A data set of thick images usually has more fully-recorded reflections, fewer partially recorded reflections, more spatial overlaps, higher X-ray background, more saturated pixels, and a lower total number of images. A fine data set has no fully recorded reflections, fewer spatial overlaps, lower X-ray background, fewer saturated pixels, more time consumed during data collection in reading out the detector between oscillations or rotations, and a much larger total number of images. Each reflection may span two or three adjacent images. Figure 5.30 is a good example of a clean oscillation exposure from a cubic insulin protein crystal [19].

5.7.8 The CMOS Detector, Pilatus 1M Detector System, and Continuous Rotation

A significant recent development in flat-plate X-ray intensity measurement technology, particularly appropriate for macromolecular crystallography, is based on the X-ray *complementary metal-oxide semiconductor* (CMOS) system.[2] The Pilatus 1M detector [20] is a CMOS with hybrid-pixel technology, a detector with over one million pixels that operates in single-photon counting mode. This detector was designed also for applications in macromolecular crystallography, and is one of the largest pixel array detectors currently in use at synchrotron sources. It consists of 18 multichip

[2] Hamamatsu Photonics KK C10158DK.

modules covering an area of about 500 cm^2 and was designed and built at the Swiss Light Source synchrotron location within the Paul Scherrer Institute, Switzerland. The modules are read out in parallel, leading to a full-frame readout time of 6.7 ms. This allows crystallographic data to be acquired in the fine-slicing mode, but with continuous rotation of the sample, not broken up into small angle oscillations, and the X-ray shutter is kept continuously in the open position during the entire data collection period. Using these techniques, the accuracy of the intensity data measurements can be improved without increasing the data collection time.

The Pilatus silicon pixel detector was used in the analysis of the crystal structure of the protein thaumatin [21]; the processing of the data produced extremely satisfactory merging *R*-factors of about 8.5% and led to a refined electron density map of the protein. The Pilatus system is marketed by Dectris [22], who also produce the Mythen detector (q.v.) for powder crystallography. Other CMOS detectors are manufactured by Dexela [23].

With shutterless data collection, images are still produced and are effectively shuttered by the instrument readout. The CCD has pixels defined by a taper of fiber optic elements and the chip is read out as a whole after the shutter is closed. For the CMOS detector each pixel has its own circuitry and is read out directly and more rapidly. Both techniques are suitable for fine-slicing [24] and the data are processed similarly.

5.7.9 Data Processing Software

A number of software packages are available for processing the data recorded by the oscillation technique. These include HKL2000 [25], which has superceded the very popular DENZO, and MOSFILM [26], and is supported by CCP4. Both of these programs have excellent indexing routines that are based on slightly different versions of the data processing software algorithm [27]. It has been recommended that it is sometimes useful to run both of these programs separately for initial assessment of a given set of data [28].

Other software packages are d*TREK [24], sold with MSC X-ray detectors, and PROTUEM,[3] a commercial program associated with Bruker detectors. The expert system ELVES [29] was developed with the intention of taking the user from data collection frames to a protein structure without human intervention. Perhaps the lessons learnt in Sect. 11.7 will encourage crystallographers to treat this option with caution.

5.7.10 Detectors and Diffractometers

The following list indicates some of the devices that are currently available for the measurement of X-ray diffraction intensities; it is not exhaustive, and some of them have been mentioned in the above discussions.

PILATUS 6M pixel CMOS detector
ADSC CCD Q-series detectors
NOIR-1 lens focused CCD detector (ALS)
MAR345 IP detector
MAR555 Flatpanel detector (TFT/Se)
MAR-MX-series tiled CCD detector
STOE IP-PSD IP detector

[3] http://www.bruker-axs.com/x8_proteum.html

SIEMENS X100A Multiwire detector
OXFORD-DIFFRACTION Xcalibur Nova CCD detector
OXFORD CRYOSYSTEMS CCD detector
ADSC Quantum 4 CCD detector
LABORATORY DESIGN GUIDE [30]
CRYO-CRYSTALLOGRAPHY [31]

5.7.11 Other Diffractometer Systems

Bruker D8 Systems
A new system from Bruker, the D8 QUEST, offers a single-crystal diffractometer with a choice of monochromatic wavelength source (Ag, Mo, Cu, or Cr). Alternatively, the IμS microfocus source is available: it consumes only 30 W but is of long life, requires no cooling and produces intensity greater than that of the traditional water-cooled rotating anode source; the diffractometer accommodates devices for low-temperature diffraction. The goniometer has a "sphere of confusion" of only 7 μm, so that the specimen is always centered in the X-ray beam. Detection is by the PHOTON 100 CMOS detector of high gain and sensitivity, and the system incorporates the APEX2 and SHELXTL computer packages for structure solution.

The companion system D8 VENTURE has substantially the same facilities as the QUEST, but provides a more spacious enclosure for the equipment. In addition, it offers either a fixed χ or a κ sample stage, giving a high degree of freedom in positioning the sample.

Rigaku SCXmini System
Among the crystallographic products offered by Rigaku, the SCXmini is the first bench-top diffractometer system; it requires minimal training and support. Data collection is carried out by the CrystalClear package, and structure solution by Oxford CRYSTALS and SHELXL. Twin crystals may be handled by the TwinSolve software.

In both of these examples of diffractometer systems, full information may be obtained from the manufacturers.[4,5]

5.8 Monochromators

In all aspects of diffraction crystallography, except for Laue diffraction, Sects. 5.4.1ff and 11.2.3ff, where a continuous spectrum is employed, intensity data are measured with radiations that are as close as possible to being monochromatic. We have seen in Sect. 3.1ff that characteristic radiation from a sealed tube can be monochromatized effectively by means of an absorption filter, but with considerable loss in intensity. In this section, we consider monochromators, which are devices designed for the production of effectively single-wavelength X-ray beams. Both the traditional sealed X-ray tube and the synchrotron source will be considered.

The Bragg equation shows that scattered X-radiation occurs at θ angles that depend upon the wavelength λ of the X-radiation. Hence, in selecting θ by reflection from a crystal plane, a monochromatic radiation may be obtained. A small scattering angle is chosen so that the loss of energy due to polarization is minimized.

[4] http://www.bruker-axs.com/chemical_crystallography.html.
[5] http://www.rigaku.com/smc/scxmini.html.

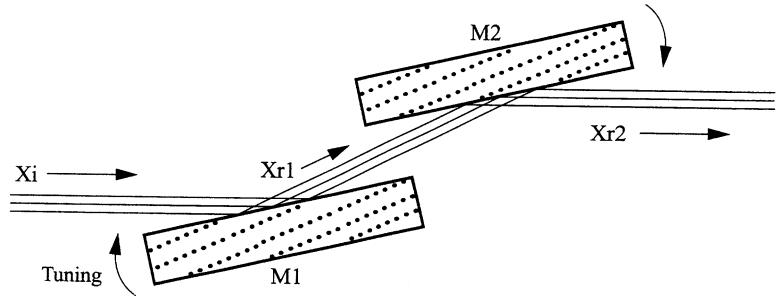

Fig. 5.31 Double-type crystal monochromator. The incident X-ray beam Xi is reflected as an essentially monochromatic component Xr1 from the first crystal M1. The second crystal M2 is set at the same angle and is therefore tuned to the same wavelength and reflects the emergent component Xr2. Tuning to a different wavelength is achieved by coupled rotation of the two crystals (*curved arrows*) and maintains the direction of incident and emergent beams, thus requiring minimal adjustment of the diffractometer. The second crystal M2 is absent in a single-type crystal monochromator

5.8.1 Single-Type Crystal Monochromators

The crystal structure of graphite consists of layers of covalently bonded, planar, hexagonal carbon rings stacked perpendicular to the *c*-axis. The stacking distance *c*/2 of 3.41 Å approximates to the van der Waals distance for carbon. This layered structure maximizes the carbon content of successive (0002) planes which thus produces an extremely strong 0002 reflection. The single-type crystal graphite monochromator operates by using this reflection as the primary beam. For a copper target, there is an approximately 20% greater loss of intensity than that suffered with a nickel filter. However, the range of selected wavelengths is very narrow and effectively monochromatic. This results in a dramatic improvement in the peak to background ratio, owing to a virtual elimination of the general background radiation produced by a sealed-tube source. Reduced heating effects resulting in improved crystal life have also been reported for some proteins.

For a monochromator tuned to wavelength λ, the harmonically related wavelengths $\lambda/2$, $\lambda/3$,... will be reflected at the same angle. This could, of course, present problems with the measured intensities, which would then relate to a composite of wavelengths. However, in practice, the harmonic wavelengths tend to be very weak in intensity and the choice of a structurally suitable monochromator material, such as graphite, will further ensure that the corresponding $I(h/n, k/n, l/n)$ values are also negligibly small.

5.8.2 Double-Type Crystal Monochromators

A disadvantage with the single-type crystal monochromator is that once tuned to select a given wavelength, the instrument cannot easily be adapted for use with a different wavelength source, because the reflecting angle will be different. This can be overcome by employing a double-type crystal monochromator, Fig. 5.31, in which the incident and emergent beam directions are the same. Tuning of the instrument is achieved by pivots fitted to both halves of the monochromator. Obviously, a further loss of intensity will be suffered with this arrangement, from the second crystal, which offsets the above advantage to some extent.

5.8.3 Monochromators for Synchrotron Radiation

The divergence of the X-ray beam from a synchrotron is small but undesirable. The effect can be corrected by using a focusing monochromator, which may be either single- or double-type. A single crystal of germanium or silicon is used for this purpose, because it has the additional advantage of a much lower bandwidth selection, or wavelength range, compared to graphite. The plane of the crystal monochromator is carefully bent in order to produce the focusing effect, which is in one direction only, forming a line focus. Further focusing may be achieved by the use of highly polished quartz or glass toroidal mirrors. Thin diamond plates, which have a high thermal tolerance, also provide excellent mirrors but suffer from the disadvantage of being extremely small [32].

5.9 Focusing Mirrors

We have noted that important features of the X-ray beam used in data collection include monochromatization, small beam divergence, high intensity, and optimal focusing. In macromolecular crystallography, a small divergence of the beam enables the use of a larger oscillation range for individual exposures without overlap of diffraction spots and consequently fewer exposures in total. It will also improve the resolution of individual spots that are close together in a crystal of large unit-cell dimensions.

X-rays can be reflected by mirrors when the angle of incidence is smaller than a critical angle, ca. 0.1°, and the use of the Franks' double focusing mirror to improve X-ray beam intensity, first introduced nearly 50 years ago [33], has been revived recently. This device consists of a pair of curved mirrors with perpendicular axes of curvature, which produces a point-focused X-ray beam, with consequent high intensity. The first mirror thus focuses the beam in one direction and the second mirror focuses the beam in the perpendicular direction to give a small, highly concentrated spot size.

The design and construction of confocal ellipsoidal mirrors for use with microfocus X-ray tubes has been described [34]. In this device, two mirrors are glued together in perpendicular arrangement at the same distance from the X-ray source, giving a fixed focus beam. Alternatively, Göbel mirrors, using parabolic focusing in a sequential double-mirror arrangement, can be used to produce a collimated parallel beam.

The advantages of the use of mirrors include an increased flux by a factor of at least three or four compared to a graphite monochromator, a narrow angular divergence and higher brilliance, a small spot size and higher brightness, a low background and some degree of monochromatization. The disadvantages are a degree of competition between monochromatization and beam flux, leading to the use of a nickel filter, for copper radiation, placed in front of the mirror, associated problems with alignment of the X-ray generator and filament with a rotating anode tube, and the requirement of a helium path to counter air-absorption, because of path lengths of approximately 200 mm.

Commercially available mirrors include the following:

- Franks' mirrors: MAR, MAC Science, Nonius XOS, and Charles Supper
- Göbel mirrors: Bruker AXS
- Confocal mirrors: Osmic's Max Flux™ (Bruker), MSC, MAR, and Nonius (AXS Confocal MaxFlux optics)

5.10 Twinning

5.10.1 Morphology of Twinning

Crystals during their formation may undergo some form of growth stress that causes them to continue the process of crystallization in other directions. The resultant material is called a twin crystal. A twinned crystal exhibits two or more orientations in one and the same crystal fragment. The portions occur in a well-defined relationship to one another: composite blocks of unit cells unite in differing orientations to form the crystal fragment. Although the portions of the fragment grow simultaneously during crystallization, it is convenient to speak of them in terms of an operation about a line, the *twin axis*, or a plane, the *twin plane*, which would bring the fragments into congruence. In some instances crystal fragments may be formed by mechanical deformation after growth, but they behave as twinned crystals. A reflection twin may be described as a *symmetric twin*, and the rotation twin as a *hemitropic twin*. Re-entrant angles are frequently an indication of twinning, whereas the interfacial angles on single crystals are salient. The plane across which two portions of a twinned crystal appear to be united is termed the *composition plane*. There is generally no physical discontinuity across this plane, merely a change of orientation; often a twinned crystal may be separated across its composition plane in order to obtain a single crystal. Another form of twinning is shown by *interpenetrant* twins, on which the crystals making up the fragment appear to have grown through one another. A composition plane is no longer possible in such cases, but the orientations of the crystals in the fragment are still related by an operation of rotation or reflection.

In some crystal fragments, the twin plane is also the composition plane; an example is the symmetric twin of gypsum, $CaSO_4 \cdot 2H_2O$. The twin may be described in terms of a rotation of 180° about the *X*-axis, (100) being the twin plane, Fig. 5.32a. The re-entrant angle is clearly evident and the specimen also exhibits an external pseudosymmetry of *mm*2, the true point-group symmetry being 2/*m*. Another form of gypsum, twined on the same law, is shown in Fig. 5.32b, but this is an example of an interpenetrant twin, with *mmm* pseudosymmetry.

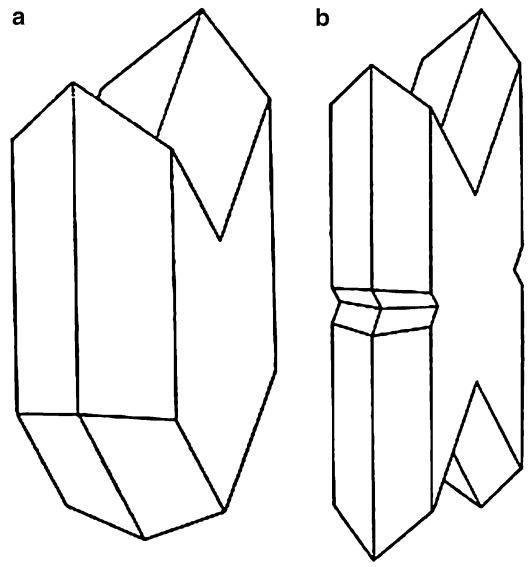

Fig. 5.32 Twinning in gypsum: (**a**) Symmetric twin of gypsum, with a (100) twin plane. (**b**) Interpenetrant twin of gypsum, also twinned on (100)

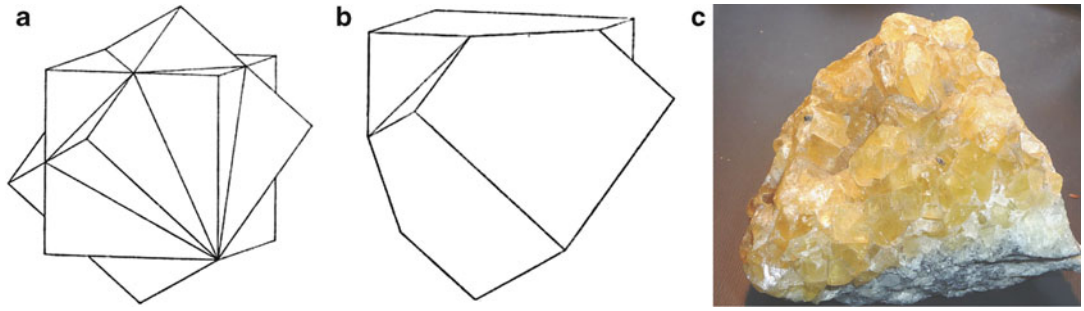

Fig. 5.33 Twinning in fluorite: (**a**) Interpenetrant twin, about (111). (**b**) Contact twin of fluorite, also twinned about (111). (**c**) Natural specimen of fluorite, showing both interpenetrant and contact twinning

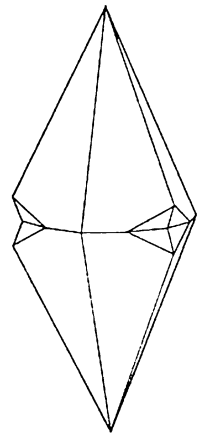

Fig. 5.34 Scalenohedral habit of calcite, $CaCO_3$, twinned about the vertical, triad axis (compare the scalenohedron in Fig. 1.3)

The mineral fluorite, CaF_2, exhibits interpenetrant twinning, Fig. 5.33a, and also contact twinning, about a threefold axis, Fig. 5.33b. Figure 5.33c is an example of naturally occurring fluorite exhibiting both interpenetrant and contact twinning.

The scalenohedral twin habit of calcite is illustrated in Fig. 5.34. It may be regarded as formed by a rotation about the vertical, triad axis, and is thus a hemitropic twin. A crystallographic axis of symmetry of even degree (2, 4 or 6) cannot function as a twin axis, because no new orientations are formed by such rotations. Similarly a crystallographic reflection plane (*m*) cannot function as the twin plane though it may, in some cases, be a composition plane.

In addition to these types of twinning, multiple twins can occur. The components may take the form of lath-like fragments, parallel to the composition plane, the whole crystal being termed a lamellar twin.

It is often possible to identify twinning under the polarizing microscope. Figure 5.35 shows two possible situations where adjacent parts of a crystal specimen are not simultaneously in extinction. Before proceeding to an X-ray examination, a single crystal may often be extracted from a twin by cutting the fragment under the microscope with a sharp, thin (razor) blade and retaining collar, Fig. 5.36. Any minute fragments adhering to the crystal can then be removed by judicious use of a solvent. The same apparatus can be used to cut crystals generally, as the occasion demands.

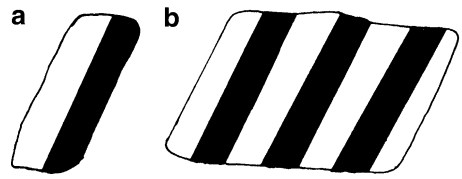

Fig. 5.35 Thin sections of twinned crystals viewed in polarized light. (**a**) Simple contact twin. (**b**) Lamellar twin. In each case, adjacent parts of the crystal are not in extinction simultaneously

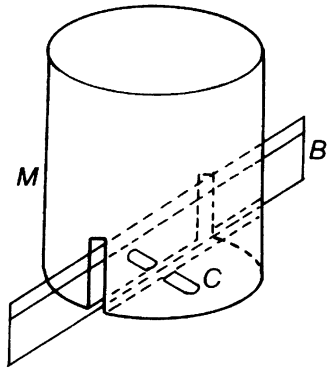

Fig. 5.36 Crystal cutting apparatus: *B* is a half razor blade, *M* is a metal or plastic collar and *C* is the crystal under examination

5.10.2 Twinning and X-Ray Diffraction

The consequence of twinning in an X-ray study is the appearance of more than one set of diffraction data for the "crystal" under examination. The two lattices may coincide, so that the two sets of reflections are superimposed in position and intensity. If the twin law is a symmetry operation of the crystal system but not of the point group of the crystal, *merohedral* twinning, such as twinning on {110} in point group $\frac{4}{m}$, occurs, and this twinning will simulate point group $\frac{4}{m}mm$, and reflections *hkl* and *khl* will be superimposed because of the apparent higher symmetry of the holosymmetric point group.

A special case of merohedral twinning is *racemic* twinning, in which a non-centrosymmetric structure is twinned with its inversion, thus leading to a superposition of reflections *hkl* and $\overline{h}\,\overline{k}\,\overline{l}$, which are not equivalent under Friedel's law, see also Sect. 7.6. The twin operation may not be of the crystal system but of a higher symmetry system, *pseudomerohedral* twinning, to which the structure approximates. A common example would be a crystal in the monoclinic system with a β-angle close to 90°. In such a case the two sets of reflections $hkl, h\overline{k}\,l, \overline{h}\,k\overline{l}$, $\overline{h}\,\overline{k}\,\overline{l}$ and $\overline{h}kl, \overline{h}\,\overline{k}l, h\overline{k}\,\overline{l}, hk\overline{l}$ each equivalent and separate under Friedel's law, but distinct in symmetry $\frac{2}{m}$, are all equivalent and superposed under symmetry *mmm*.

In merohedral and pseudomerohedral twinning, the X-ray diffraction pattern can normally be indexed on a single unit cell, but indications of twinning arise in space group determination, intensity statistics or in the structure determination proper. Where the components do not overlap, *non-merohedral* twinning, problems with the unit-cell determination may arise, leading to a doubling of one axis or more.

One way of avoiding problems with twinning may be by its early recognition. Interpenetrant twins may be recognized under the microscope by their shape, and their use avoided. Contact twins can

often be determined with the microscope under polarized light. The two portions of the fragment may appear in extinction or show polarization colors at different positions of the microscope stage. If the boundary of two crystals comprising the fragment can be recognized, the crystal may be cut using the simple apparatus shown in Fig. 5.36: then one is again dealing with a single crystal.

The SHELX structure solution program (see Appendix D) incorporates facilities (BASF and TWIN) that enable tests to be carried out in the penultimate stages of least-squares refinement, and interesting accounts of twinning may be found on the web site references below [35, 36].

5.11 Problems

5.1. Crystals of KH_2PO_4 are needle-shaped and show straight extinction parallel to the needle axis. A Laue photograph taken with the X-rays parallel to the needle axis shows symmetry $4mm$.
   (a) What is the crystal system and Laue group, and how is the optic axis oriented?
   (b) Describe and explain the appearance between crossed Polaroids of a section cut perpendicular to the needle axis.
   (c) What minimum symmetry, would be observed on both general and symmetric oscillation photographs taken with the crystal mounted on the needle axis?

5.2. Crystals of acetanilide (C_8H_9NO) are brick-shaped parallelepipeda, showing straight extinction for sections cut normal to each of the three edges of the "brick"
   (a) What system would you assign to the crystals?
   (b) Allocate suitable crystallographic axes.
   (c) What minimum symmetry would be shown by general oscillation photographs taken, in turn, about each of the three crystallographic axes?
   (d) What symmetry would an oscillation photograph exhibit where the crystal is oscillating about the a axis such that b is parallel to the X-ray beam at the center of the oscillation range?

5.3. Crystals of sucrose show the extinction directions indicated on the schematic crystal drawing of Fig. P5.1; the arrows indicate the directions of the cross-wires at extinction.
   (a) To what crystal system does sucrose belong?
   (b) How are the morphological directions, p, q, and r related to the crystallographic axes?
   (c) How would you mount the crystal in order to test your conclusions with (i) Laue photographs, in a single mounting of the crystal, and (ii) oscillation photographs? In each case, indicate the symmetry you would expect the photographs to exhibit in the orientations you have chosen.

5.4. A cubic crystal of side $a = 5.0$ Å is mounted on a flat-plate Laue camera so that one axis (b or c) lies along the rotation axis and a is inclined to the X-ray beam at an angle $\phi = 70°$. If the crystal is irradiated with an X-ray beam possessing the wavelength range 0.2–2.5 Å, determine

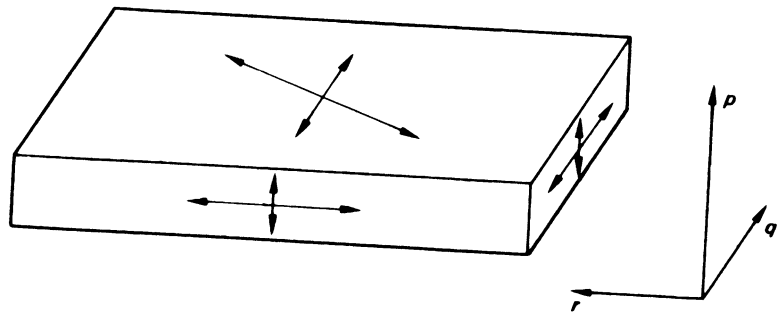

Fig. P5.1 Crystal section of sucrose, showing extinction directions

the highest order $h00$ reflection that can be recorded. If the cassette is placed at a distance R of 60 mm from the crystal and the film plate is 125 mm^2, determine whether this reflection will be recorded and, if so, find its coordinates on the film in mm.

5.5. A Laue photograph of a protein crystal is recorded on a pack of two films separated by black paper. A particular reflection hkl for a wavelength λ in the "white" radiation is overlapped on the films by the reflection $2h$, $2k$, $2l$ for the wavelength $\lambda/2$. The black paper transmits 65% of the radiation of shorter wavelength and 35% of the longer wavelength radiation. If the relative intensity of the composite reflection measured on the film first to receive the reflected beam is 300 but only 130 on the second film, what are the relative intensities of the two reflections on the first film?

5.6. β-Zinc sulphide, ZnS, crystallizes in space group $F\bar{4}3m$, with $a = 5.41$ Å. A flat-plate Laue photograph, taken with a crystal-to-film distance of 30.00 mm, exhibits symmetry $2mm$.
(a) What was the direction of the incident beam in the crystal?
(b) The horizontal m line on the film displays two pairs of reflections, symmetrically disposed about the center of the film. The two reflections of the outer pair are 77.5 mm apart, and the inner pair 43.5 mm apart. For each reflection in the two pairs, find (i) the Bragg angle θ, (ii) the indices hkl and (iii) the wavelength producing each spot.

5.7. Oscillation photographs of manganese carbonate, $MnCO_3$, taken about three mutually perpendicular axes, and Laue photographs along the same three axes gave the following results ($\lambda = 1.5418$ Å):

Axis	1	2	3
Layer line	8	4	2
Distance/mm from zero layer	38.40	33.63	25.40
Laue symmetry	$3m$	m	2

Determine the unit-cell dimensions and the Laue group of the substance; the diameter of the oscillation camera was 60.00 mm.

5.8. The 0002 reflection from a single crystal of graphite can be used to obtain monochromatic X-radiation from its (0001) plane. If the c dimension of graphite is 6.696 Å, calculate the appropriate Bragg angle for reflection of (a) Cu $K\alpha$ ($\lambda = 1.5418$ Å) and (b) Mo $K\alpha$ ($\lambda = 0.7107$ Å) radiation at which the crystal monochromator must be set.

5.9. An orthorhombic crystal was set in a random orientation on an automatic four-circle single-crystal X-ray diffractometer. A peak search led to a primitive reciprocal unit cell of dimensions $a^* = b^* = 0.239$, $c = 0.184$, $\alpha^* = \beta^* = 90$, $\gamma^* = 152.4°$, using Mo $K\alpha$ radiation ($\lambda = 0.7107$ Å). Determine the transformation matrix to convert the "diffractometer" cell to the true cell, which was known from photographs to have the approximate dimensions $a = 3.1$ Å, $b = 12.5$ Å, and $c = 3.9$ Å, (a) in real space and (b) in reciprocal space.

5.10. (a) The diffraction pattern from a protein crystal is required to be recorded on an image plate having a diameter of 345 mm. If the resolution d_{min} required is 1.0 Å and an X-ray wavelength of 1.05 Å, is being used, calculate the furthest distance R in mm that the plate can be set from the crystal.
(b) What would happen to the diffraction pattern in (a) if the plate were set 10 mm nearer to the crystal?
(c) What would happen to the diffraction pattern in (a) if the plate were set 10 mm further from the crystal?

5.11. Refer to Fig. P5.2a–c. Each figure poses a problem relating to X-ray records.

Oscillation Angle

The 3 diffraction images below were recorded from the same crystal using the same X-ray wavelength, but different oscillation angles. Underneath each image write in the corresponding oscillation angle. The choices are 0.10°, 1.00°, and 5.00°.

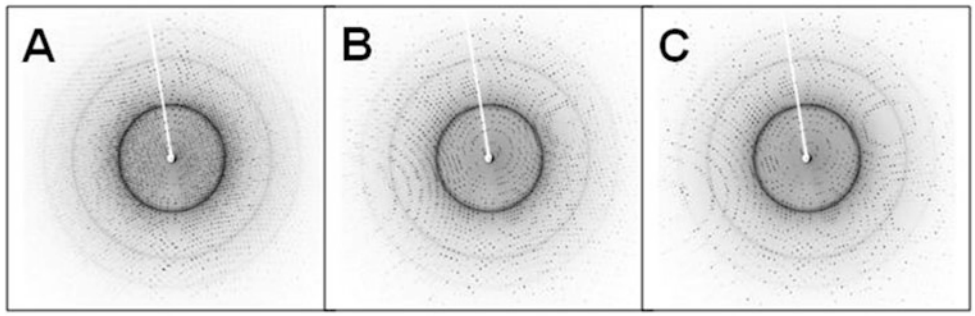

Distance

The 3 diffraction images below were recorded from the same crystal using the same X-ray wavelength, but different crystal-to-detector distances. Underneath each image write in the corresponding crystal-to-detector distance. (80, 250, or 450 mm)

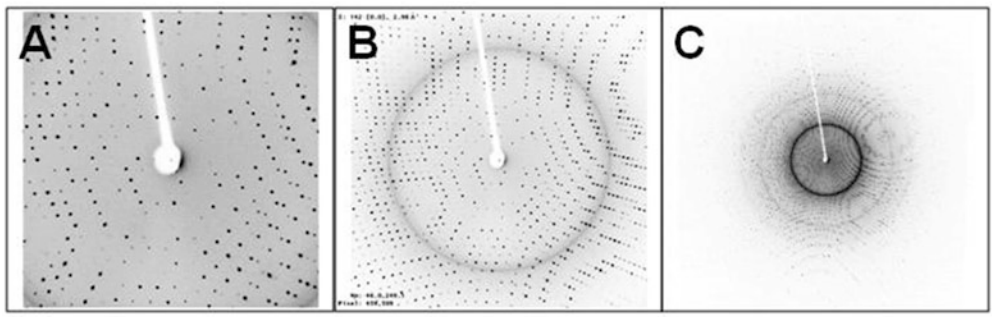

Time

The 3 diffraction images below were recorded from the same crystal using the same X-ray wavelength, but different lengths of exposure. Underneath each image write in the corresponding length of exposure. The choices are 12 s, 60 s, and 300 s.

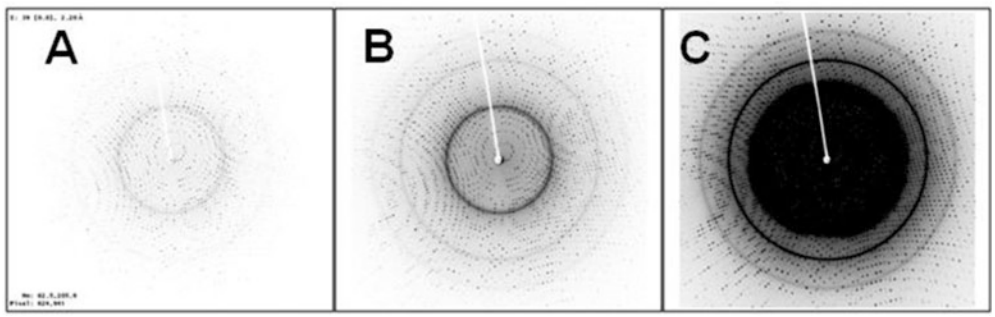

Fig. P5.2 Diffraction images from a given crystal, with a fixed wavelength, but with varying oscillation angle, crystal–detector distance, and exposure time

References

1. Bibliography, Gay (1967); Hartshorne and Stuart (1970)
2. See Bibliography, Buerger MJ (2009)
3. Ladd M, Palmer R (2003) Structure determination by X-ray crystallography, 4th edn. Kluwer Academic, New York
4. http://www.bruker-axs.com/spacegroupdetermination.html
5. See Bibliography, Jeffrey
6. Arndt UW, Wonacott AJ (eds) (1977) The rotation method in crystallography. North-Holland, Amsterdam
7. Mar Research (MAR IP) Norderstedt, Germany
8. Miyahara J et al (1986) Nucl Instrum Methods A246:572
9. Boyle W, Smith G (1970) Charge coupled semiconductor devices. Bell Syst Tech J 49:587
10. Einstein A (1905) Ann Phys 17:132
11. Gruner SM (1994) Curr Opin Struct Biol 4:765
12. Westbrook EM, Naday I (1987) Methods Enzymol 276:244
13. Jones C (2001) Chem Commun 2293
14. Deacon A et al (1997) J Chem Soc Farad Trans 93:4305
15. Walter RL et al (1995) Structure 3:835
16. http://www.nonius.com
17. http://www.bruker-axs.com
18. Oxford Cryosystems, http://www.oxcryo.com
19. Prince SM, Bryant PK (private communication) Manchester University
20. Brönnimann Ch et al (2004) Synchrotron Radiat News 17:23
21. Brönnimann Ch et al (2006) J Synchrotron Radiat 13:120–130
22. http://www.dectris.ch/sites/products.html
23. http://www.dexela.com
24. Plugrath JW (1999) Acta Crystallogr D55:1718
25. Otwinowski Z, Minor W (2001) 'Denzo' and 'Scalepack 211'. in Arnold, E et al. (2012) (eds) International Tables for Crystallography, vol. F, I.U.Cr.
26. Leslie A (1993) Data collection and processing. In: Sawyer L, Isaacs N, Bailey S (eds) Proceedings of the CCP4 study weekend. Daresbury Laboratories, Warrington, UK, pp 44–51
27. Rossmann MG, van Beek CG (1999) Acta Crystallogr D55:1631
28. Sanderson MR (2007) Macromolecular crystallography conventional and high-throughput methods, Chapter 5. Oxford University Press, Oxford
29. Yarris Lynn, lcyarris@lbl.gov
30. http://www.xtl.ox.ac.uk/equip.html
31. http://people.mbi.ucla.edu/sawaya/m230d/Data/data.html
32. Freund AK (1996) Structure 4:155
33. Franks A (1955) Proc Phys Soc London B68:1054
34. Bloomer AC, Arndt UW (1999) Acta Crystallogr D55:1672
35. http://www.lcm3b.uhp-nancy.fr/mathcryst/twins.htm
36. http://xrayweb.chem.ou.edu/notes/twin.html
37. http://www.bruker-axs.com/d8_advance.html
38. http://www.rigaku.com/downloads/journal/Vol12.2.19 95/raxisiv.pdf

Bibliography: Crystal Optics

Gay P (1967) An introduction to crystal optics. Longmans, London
Hartshorne NH, Stuart A (1970) Crystals and the polarising microscope. Arnold, London

X-Ray Scattering and Reciprocal Lattice

Arndt UW, Wonacott AJ (eds) (1977) The rotation method in crystallography: data collection from macromolecular crystals. North-Holland, Amsterdam

Buerger MJ (2009) X-ray crystallography, 11th edn. Wiley, New York
Jeffrey JW (1971) Methods in X-ray crystallography. Academic, London
Woolfson MM (1997) An introduction to X-ray crystallography, 2nd edn. Cambridge University Press, Cambridge

Interpretation of X-Ray Diffraction Photographs

Henry NFM, Lipson H, Wooster WA (1960) The interpretation of X-ray diffraction photographs. Macmillan, London
Jeffery JW (1971) Methods in X-ray crystallography. Academic, London

Precession Method

Buerger MJ (1964) The precession method. Wiley, New York
Ladd MFC, Palmer RA (2003) Structure determination by X-ray crystallography, 4th edn. Kluwer Academic, New York

Diffractometry

Arndt UW, Willis BTM (1966) Single crystal diffractometry. Cambridge University Press, Cambridge

Cryo-Crystallography

Ealick S et al. Cryocrystallography: a practical approach http://people.mbi.ucla.edu/Sawaya/m230d/Data/data.htmlhtml

Macromolecular Crystallography

Carter CW Jr, Sweet RM (eds) (1997) Macromolecular crystallography. Academic, New York
Arnold, E et al. (2012) (eds) International Tables for Crystallography, vol. F, I.U.Cr.

Data Collection

Evans PR (1999) Acta Crystallogr D55:1771
Dauter Z (1999) Acta Crysatallogr D55:1703

Data Collection Services

The EPSC National Data Collection Service (University of Southampton) will collect, process, and optionally solve crystal structures (but there's not much fun in that) for clients who supply suitable crystals. In a recent use of this service the following facilities were used

Diffractometer: Nonius Kappa CCD Area Detector (ϕ scans and ω scans to fill the asymmetric unit sphere)
Cell determination: DirAx (Duisenberg AJM (1992) J Appl Crystallogr 25:92)
Data collection: Collect (Data collection software, Hooft R, Nonius BV (1998))
Data reduction and cell refinement: *Denzo* (Otwinowski Z, Minor W (1997) Methods Enzymol 276); Macromol Crystallogr, loc. cit.
Absorption correction: *SORTAV* (Blessing RH (1995) Acta Crystallogr A51:33); idem., J Appl Crystallogr 30:421 (1997)
Structure solution: SHELXS-97 (Sheldrick GM (1990) Acta Crystallogr A46:467)
Structure refinement: SHELXL-97 (Sheldrick GM (1997) University of Göttingen)
Graphics: *ORTEP3 for windows* (Farrugia LJ (1997) J Appl Crystallogr 30:365)